Available online at www.sciencedirect.com
SCIENCE DIRECT®
Radiation Physics and Chemistry 70 (2004) 149–172
Radiation Physics and Chemistry
www.elsevier.com/locate/radphyschem

Higher-order processes in X-ray photoionization and decay

R.W. Dunford, E.P. Kanter, B. Krässig, S.H. Southworth*, L. Young

Argonne National Laboratory, Argonne, IL 60439, USA

Abstract

Over the past decade, modern synchrotron radiation sources have provided continuously tunable, intense well-collimated beams of hard X-rays. Our group has exploited such beams, in the energy range 2–100 keV, to study higher-order processes in atomic photoionization and vacancy decay which were hitherto difficult to observe and we review five specific examples of that work here. These topics include high-energy photoionization of helium, nondipolar photoionization, double K-shell ionization, two-photon decays of inner-shell vacancies, and nuclear excitations by electronic transition.

PACS: 32.80.Fb; 32.80.Hd; 32.30.Rj; 23.20.Nx

Keywords: X-ray photoionization; He photoionization; Double-K ionization; Nondipole photoionization; Two-photon decay; Nuclear excitation by electronic transition (NEET)

1. Introduction

In this contribution we describe some recent experiments performed at the Argonne Advanced Photon Source (APS) and the Brookhaven National Synchrotron Light Source (NSLS) which investigate photoabsorption processes in the energy range of 2–100 keV. The basic physics of the atomic photoelectric effect in the X-ray regime (Pratt et al., 1973; Crasemann, 1996) and of inner-shell vacancy decay (Crasemann, 1985) is well established. However, detailed studies can highlight aspects of X-ray/atom interactions beyond the commonly used independent-particle and dipole approximations. The intense, tunable, polarized, and focused beams of hard X rays provided at synchrotron light sources enable detailed studies of X-ray/atom interactions, e.g., measurements that are differential in energy and angle or detect emitted X rays in coincidence. The access to very high X-ray energies has enabled studies of rare decay processes, previously studied only with radioactive sources. Here we describe several experiments using synchrotron X rays that probe higher-order processes and provide data to test and develop theory.

We start with the simplest non-trivial atom, helium, and examine both the double ionization probability and the total ionization cross section. The experiments required extreme care due to the small cross section, approximately one barn, and the fact that two distinct ionization mechanisms, photoeffect and Compton scattering, operate at keV photon energies. The experimental results on the helium atom serve as a testbed for advancing dynamical many-body methods. Because of the closely correlated 1s electrons in helium, theoretical descriptions must a priori include ground-state and final-state correlation in order to achieve reasonable agreement with experiment. We next discuss the X-ray photoionization process in more complex atoms, argon and krypton, between 2 and 22 keV. Here, the photoeffect dominates both Compton and Rayleigh scattering and photoionization dynamics can be studied by observation of ejected photoelectrons. The simplest model of atomic photoionization invokes the dipole approximation for the radiation-field/atom interaction, and our experimental work measuring photoelectron asymmetries probes nondipole interactions. Special measurement geometries are required to isolate the

*Corresponding author.
E-mail address: southworth@anl.gov (S.H. Southworth).

0969-806X/$ - see front matter © 2004 Elsevier Ltd. All rights reserved.
doi:10.1016/j.radphyschem.2003.12.010

nondipole contribution. Combining our results with theoretical efforts, we are able to establish the degree of complexity in the atomic description that is necessary to describe the measured nondipole asymmetries.

We then move on to studies of a less common process, namely the production of double-K vacancies. Relative to the primary photoionization that creates a single K-vacancy, the probability of creating double-K vacancies is $\approx 10^{-2}$ at $Z = 2$ and is further reduced by a factor which scales roughly as $1/Z^2$ for higher Z. The appearance of the double-K vacancy state is a signature of electron correlation, and these studies are closely related to the double ionization of helium discussed in Section 2. We consider the optimization of experimental methods to observe double-K vacancy production in low-, medium- and high-Z atoms. The final two sections concentrate on rare decay modes of inner-shell vacancies, namely, two-photon decay and nuclear excitation by electronic transition (NEET). Both of these decay modes are very rare. Relative to the ''normal'' decay mode, Kα X-ray emission, two-photon decays are typically 4–8 orders of magnitude lower and NEET usually even smaller. Two-photon decay provides an important complementary tool for testing atomic structure calculations in that summation over a complete set of virtual states is required to compare to experiment. We describe an experiment in Au which is the first to use synchrotron radiation to observe two-photon decay in a neutral atom. Finally, we report on a search for NEET in ^{189}Os. The result of this search was to place a more stringent limit on the NEET probability and to stimulate more accurate calculations and a better understanding of the NEET mechanism.

Throughout these experimental studies runs the theme of going beyond the simplest approximations that are usually made to describe X-ray processes. In fact, most of the processes discussed here are *only* allowed in higher-order treatments. One will find a close interplay between our experiments, which we intend to motivate theoreticians, and the development of a more complete description for X-ray interactions with atoms.

2. X-ray ionization of helium

X rays with keV energies interact only very weakly with helium atoms. Nonetheless, this interaction is one of the most fundamental processes in atomic physics. It is the ideal system to study electron exchange and correlation effects in X-ray–matter interactions. Accurate cross sections for this interaction are needed to model the absorption of X rays in the interstellar matter which is mainly made up of light elements (e.g. Verner et al., 1996). In a previous issue of this journal, Cooper (1996) gave a review and an assessment of the then available measured and calculated cross sections that contribute to the attenuation of photons in helium. Here, we will attempt to supplement that picture with recent experimental and theoretical findings.

Single ionization is the most likely outcome of the X-ray–helium interaction. Double ionization amounts to less than two percent of total ionization of helium in the keV-energy regime. Fig. 1 displays the energy dependence of the three main interaction mechanisms in helium as tabulated by the XCOM data base (Berger et al., 1999). Nonrelativistically, the photoabsorption cross section falls off with an $(\hbar\omega)^{-7/2}$ power law. Below 6 keV, ionization proceeds predominantly through the absorption of the X-ray photon. Above 6 keV, Compton scattering takes over as the main mechanism for ionization. The total incoherent scattering cross section also contains a small nonionizing fraction, Raman scattering. Coherent scattering, which contributes to the attenuation cross section but not to ionization, is always smaller than the total ionization cross section. Near 6 keV the coherent Rayleigh scattering process has its strongest relative contribution to the attenuation of X-rays in helium, measuring approximately 30%. Above 6 keV the contribution of Rayleigh scattering decreases steadily with increasing energy.

The process of instantaneous double ionization, specifically in helium, but also in heavier systems (see Section 4), has been the subject of manifold theoretical and experimental endeavours (McGuire et al., 1995). More experimental and theoretical efforts have gone into studying double ionization of helium by photoabsorption than into double Compton ionization. On the experimental side this imbalance is caused by the small magnitude of the ionization cross section in the energy region where Compton scattering becomes important. Simple ion counting techniques cannot distinguish between absorption and Compton scattering

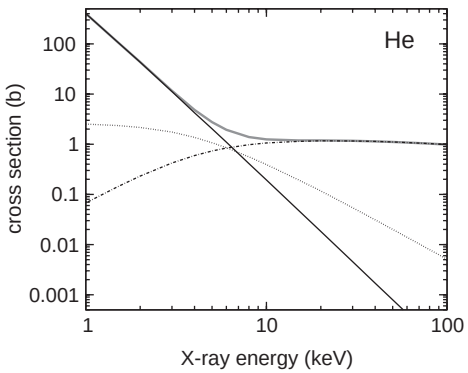

Fig. 1. The X-ray–helium interaction cross sections according to the XCOM data base (Berger et al., 1999). Solid line, photoabsorption; chain curve, incoherent scattering; dotted curve, coherent scattering; thick shaded curve, X-ray attenuation.

in the energy region where both processes contribute to ion production (Samson et al., 1993). The theoretical calculations for double ionization in Compton scattering, which is a second-order process, are inherently more difficult to perform than the dipole approximation calculations for photoabsorption.

The knowledge of the X-ray cross sections for these interaction mechanisms comes mainly from theoretical calculations. Absolute measurements exist only for the attenuation cross section, which is the sum of the cross sections for all the above interactions. A compilation of available attenuation measurements before 1988 along with the results of calculations and relevant references can be found in Saloman et al. (1988). Azuma et al. (1995) reported a large number of new attenuation data points for helium in the 3–14 keV X-ray energy range. In a measurement of the differential scattering cross section, Ice et al. (1978) obtained absolute values of total photon scattering at 6 keV for two different scattering angles. Other experimental cross section determinations are usually relative measurements: double ionization relative to single ionization, scattering relative to absorption, angular distribution measurements, etc.

In this section we will discuss experimental results for two relative quantities of X-ray ionization in helium: the ratio of double to single ionization (2.2), and the ratio of Compton scattering to photoabsorption (2.3). Using a consistency check with theoretical predictions we will be able to draw conclusions about the absolute magnitudes of the total ionization cross sections. Before turning to the results we will discuss some experimental aspects of these measurements.

2.1. Experimental issues

In the 3–12 keV X-ray energy window both photoabsorption and Compton scattering are significant in the production of helium ions. When simply counting ions, the observed ratio of double-to-single ionization in this energy range is a cross-section weighted sum of the absorption double-to-single ratio and the Compton double-to-single ratio.

Samson et al. (1994) demonstrated that ions created by photoabsorption and ions created by Compton scattering can be distinguished by virtue of their different recoil momentum distributions. Spielberger et al. (1995) perfected this idea by applying cold target recoil ion momentum spectroscopy (COLTRIMS, Ullrich et al., 1997) in their measurement. In our own measurements of the two quantities discussed above we also used the COLTRIMS technique in an experiment performed at the undulator beamline 12-ID operated by the Basic Energy Sciences Synchrotron Radiation Center (BESSRC) at the APS (Krässig et al., 1999). Briefly, the COLTRIMS apparatus consists of a time-of-flight ion mass analyzer with a position-sensitive detector used in conjunction with a supersonically cooled atomic beam as a target. For each ionization event the time-of-flight of the ion relative to the singlet bunch pattern of the storage ring and the impact location on the detector are recorded on tape for off-line analysis. Displacements of the detected ions from the center of the detector and shifts from their nominal flight times are proportional to the recoil momentum that the initially cold ions receive in the ionization process. In photoabsorption the recoil momentum of the ion is equal and opposite to the momentum of the emitted photoelectron(s). Compton scattering on the other hand is mainly a binary encounter between the X ray and an electron and the ion receives negligible momentum during the ionization process. In this way events from photoabsorption and Compton scattering can be distinguished in the experiment.

As an example Fig. 2 shows data from our experiment for single ionization in helium taken with 8-keV X rays. The coordinates are the polar angle and magnitude of the ion recoil momentum in the laboratory frame. The direction of the X-ray beam is indicated by the arrow. The events in the center with very small momenta are ions created by Compton scattering. The events on the surrounding ring are the ions created by photoabsorption. The radius of the ring corresponds to the momentum of the emitted photoelectron (24.21 a.u.). The point density in the ring of ions from photoabsorption reflects the nondipolar forward–backward asymmetry of the photoelectron emission (see Section 3).

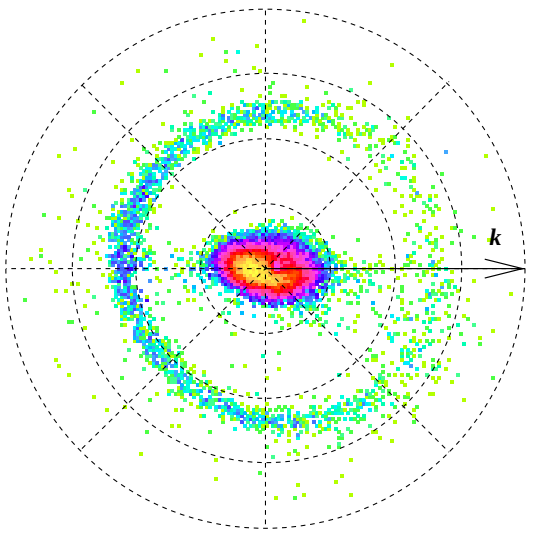

Fig. 2. Polar plot of the recoil momenta for He^+ ions measured for 8-keV X rays in the laboratory frame. The direction of the X-ray beam is denoted by the vector $\boldsymbol{k}$, grid units are 10 a.u. Compton events are in the center, photoabsorption events are on the surrounding circle. See text.

More electrons are emitted into the forward direction, therefore, more ion recoil momenta are found pointing in the backward direction. Furthermore, the ring of photoabsorption events is displaced by 2.14 a.u. in the direction of the photon beam, which is the momentum of the X-ray photon absorbed by the ion. For double ionization one obtains a similar figure, but 50 times less intense. From a practical standpoint, the Compton events in experimental data sets as in Fig. 2 are cleaner and less affected by underlying background or dark counts than the photoabsorption events, which are spread out over a much larger area of the detector surface and the time-of-flight spectrum and consequently have a poorer signal-to-noise ratio.

2.2. X-ray double ionization of helium

One of the issues discussed in the literature is the high-energy asymptotic limit for the ratio of double-to-single ionization. This asymptotic limit can be calculated more easily than the value of the ratio for a given energy. It was the goal of experimental determinations to confirm the theoretical prediction and to establish how high in X-ray energy one must go in order to be in the asymptotic region.

Photoabsorption and Compton scattering have different high-energy asymptotic behaviors in the ratio of double-to-single ionization. This high energy behavior is typically thought of in the framework of the ''sudden approximation'' (Åberg, 1970). It means that one of the electrons is instantaneously removed from the atomic shell during the X-ray–atom interaction and the other electron then has a certain probability of being promoted into the continuum as a result of the relaxation of the ionic potential. This mechanism is also called ''shake-off'' in the literature. The energy distribution of such double ionization events shows only very fast and very slow electrons. The ion recoil momentum arises predominantly from the emission of the fast electron. Åberg (1970) found that the calculated magnitude of the asymptotic ratio depends critically on the inclusion of electron correlation in the initial state wave function. The difference between photoabsorption and Compton scattering arises from the fact that in order to be able to absorb the photon momentum, the electron must be deep in the atomic potential near the nucleus. The photoelectron is expelled with most of the excess energy and the ion recoils from the emission. In Compton scattering there is no such restriction and the 'first' electron can come from anywhere in the atom. Thus, in the framework of the sudden approximation the high-energy ratio of double-to-single ionization in helium for Compton scattering R_C is about half of the corresponding value R_P for photoabsorption (Surić et al., 1996). The sudden approximation asymptotic limit for photoabsorption can be calculated to high accuracy, $R_P = 0.01645$ (Forrey et al., 1995; Krivec et al., 2000). While it is justified to regard keV photoabsorption leading to a keV photoelectron as close to the ''sudden'' scenario, the same is not a priori clear for Compton scattering because even for very high X-ray energies the momentum transfer to the electron can be small for forward scattered X-rays.

In the context of this section the terms ''sudden approximation'' and ''shake-off'' denote the same mechanism and imply proper accounting for ground state correlations. Please note that the term ''shake-off'', abbreviated SO, is also used as a descriptor for a certain diagram in many body perturbation theory (MBPT), which is distinct from the ''ground state correlation'' diagram, GSC (see Section 4.1, Fig. 11).

The interplay between photoabsorption and Compton scattering in the double-to-single ionization ratio of helium already manifested itself in the data of Sagurton et al. (1995) and Levin et al. (1996) which did not distinguish between the two interactions. The ratio was seen to approach the photoabsorption asymptotic value near 3 keV, but beyond this energy the ratio first dropped to lower values and then rose again to values near 1.6% at energies where photoabsorption has become insignificant. More recent measurements with the capability of separating photoabsorption and Compton events have helped to interpret these findings. It is instructive to look first at the published results of the helium double-to-single ionization ratio by Compton scattering shown in Fig. 3a. The measurements of Spielberger et al. (1995, 1996, 1999), Morgan and Bartlett (1999), and our group (Krässig et al., 1999) used techniques which allowed for the separation of Compton events from photoabsorption events. The results of Levin et al. (1996), Samson et al. (1996), Wehlitz et al. (1996), and Becker et al. (1999) did not distinguish the two interactions, but the data points included in the figure are at high enough energies where photoabsorption is less than 10% of total ionization. Fig. 3a also contains the published theoretical predictions for the Compton double-to-single ionization ratio in helium. Of these calculations the MBPT calculation of Bergstrom et al. (1995) has the best resemblance to the experimental findings. This calculation extends only up to 20 keV where it seems to deviate from experiment more than at lower energies. Towards the high energy end of the figure the measurements of the Compton double-to-single ratio flatten out to a value just below 1%. The calculation reported by Spielberger et al. (1999), with values of 0.9% and 0.87% at 40 and 100 keV respectively, also seems to indicate a very slow convergence to the theoretical high-energy asymptotic limit of 0.8% marked by the dotted line.

It can be seen from the trend in Fig. 3a that the Compton double-to-single ratio below about 7 keV is smaller than one percent. This explains why the

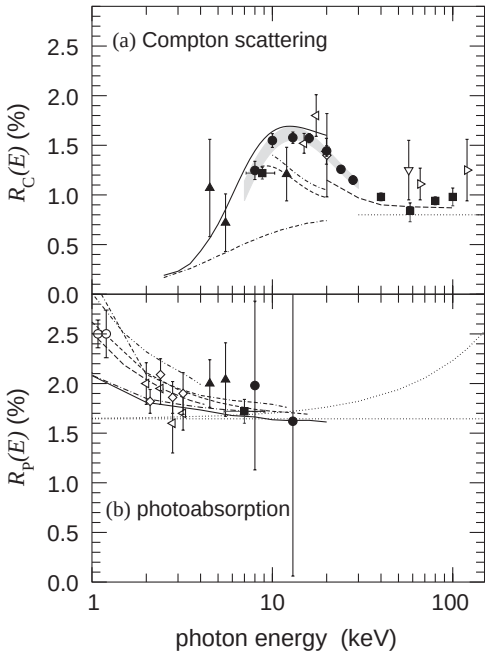

Fig. 3. The ratio of double-to-single ionization in helium. (a) Compton scattering. Solid circles, Krässig et al. (1999); solid squares and long-dash line, Spielberger et al. (1995, 1996, 1999); solid triangles, Morgan and Bartlett (1999); left open triangles, Levin et al. (1996); open diamond, Samson et al. (1996); inverted open triangle, Wehlitz et al. (1996); right open triangles, Becker et al. (1999); solid line, Bergstrom et al. (1995); short dash and dash–dotted lines, Andersson and Burgdörfer (1994a); dash–dash–dotted line, Surić et al. (1994); dotted line, theoretical asymptotic limit. (b) Photoabsorption. Solid circles, this work; solid square, Spielberger et al. (1995); solid triangles, Morgan and Bartlett (1999); open circles, Berrah et al. (1993); left open triangles, Levin et al. (1996); open diamonds, Sagurton et al. (1995); solid curve, Hino et al. (1993); dash–dotted curve, Kheifets and Bray (1998); long dash curve, Pan and Kelly (1995); short dash curve, Qiu et al. (1998); dash–dash–dotted curve, Kornberg and Miraglia (1993); dash–dot–dot curve, Drukarev and Trzhaskovskaya (1998); dotted lines, theoretical asymptotic limits with and without (horizontal) the quasi-free contribution.

measurements of the combined Compton plus photoabsorption double-to-single ionization ratio (Sagurton et al., 1995; Levin et al., 1996) saw the ratio drop from 2% at 2 keV X-ray energy to below the theoretical photoabsorption asymptotic limit of about 1.6% near 5 keV. At 5 keV the Compton cross section is about 60% smaller than the photoabsorption cross section, but it contributed relatively more singly charged ions than photoabsorption to the combined ratio. The approach to the asymptotic limit of the photoabsorption double-to-single ratio is masked by the onset of Compton scattering and can therefore not be observed without distinguishing between the two interaction processes.

Several groups reported measurements aimed at the photoabsorption high-energy double-to-single ionization ratio. Some of these were at a low enough energy, less than 3 keV, so that Compton scattering may not have had as much influence (Levin et al., 1991; Berrah et al., 1993) as in the 3–12 keV energy region (Levin et al., 1993; Sagurton et al., 1995; Levin et al., 1996). The measurements of Spielberger et al. (1995) and Morgan and Bartlett (1999) separated Compton and photoabsorption events and produced separate ratios for the two interactions.

The experimental double-to-single ionization results that can be safely attributed to just photoabsorption are shown in Fig. 3b. The horizontal dotted line near 1.6% shows the theoretical asymptoptic limit in sudden approximation. The measurements seem to indicate that the ratio is still above 2% for energies below 2 keV. The measurement of Spielberger et al. (1995), performed with the unmonochromatized broad band output of an undulator, quotes the smallest error bar and is in good agreement with the theoretical asymptotic limit, $R_P = (1.72 \pm 0.12)\%$ for $7.0^{+2.1}_{-1.6}$ keV. Our own measurements, $R_P(8\,\text{keV}) = (1.98 \pm 0.85)\%$ and $R_P(13\,\text{keV}) = (1.62 \pm 1.56)\%$ are consistent with this limit but they have very large error bars due to the poor signal-to-noise ratio in these measurements.

Some representative theoretical calculations of the double-to-single photoabsorption ratio are also shown in Fig. 3b. Most converge on the asymptotic limit. Above 2 keV the experimental error bars do not allow to distinguish between calculations. The two data points of Berrah et al. (1993) seem to favor the calulations of Pan and Kelly (1995) and Qiu et al. (1998). The former calculation and the calculation of Hino et al. (1993) are both performed in MBPT, yet they differ by an appreciable amount below 2 keV. In the low-energy regime, the results of Hino et al. (1993), particularly in acceleration form, are closer to recent high-quality experimental data (Samson et al., 1998) than those of Pan and Kelly (1995). It should be noted that any differences in the double-to-single ratio between different calculations may not just arise from the respective calculations of the double ionization cross section, which in most cases is the main focus in those papers, but also from the single ionization result. The situation of helium single ionization cross sections will be addressed in Section 2.3.

It was recently pointed out that the notion in photoabsorption of a high-energy asymptotic value for the double-to-single ionization ratio is only valid in the sudden approximation picture or in dipole approximation. In higher order, there is the possibility of a "quasi-free" process in which the energy and momentum of the X-ray photon are transferred to the two electrons, rather than to one electron and the nucleus (Drukarev, 1995; Kornberg and Miraglia, 1999; Surić et al., 2003), see also

Amusia et al. (1975). This process is predicted to lead to an increase of the photoabsorption double-to-single ratio linear with energy. It is further predicted to lead to the emission of two photoelectrons with near equal energies, and to a nucleus with negligible recoil momentum. The projected ratio with the quasi-free effect is also shown in Fig. 3b as a dotted line (note the logarithmic abscissa).

The aforesaid has consequences for the interpretation of the experimental double ionization data measured with the COLTRIMS technique. Strictly, one should therefore consider those doubly ionized ions with recoil momentum as photoabsorption "shake-off" events, and those ions with no recoil momentum as Compton events plus photoabsorption "quasi-free" events. However, within the current error limits of the ratio measurements, the presence or absence of the quasi-free effect cannot be discerned.

2.3. X-ray total ionization of helium

The total ionization cross section in the region of present interest is 98% single ionization. Its accuracy therefore depends first and foremost on the accuracy with which single ionization is known. The single ionization process is generally considered to be well understood. In contrast to this popular wisdom, comparison between various tabulations for the photoabsorption and scattering cross sections (Veigele, 1973; Hubbell et al., 1975; Henke et al., 1993; Chantler, 1995) reveals up to double-digit percentage differences between them.

The tabulations of the cross sections for photoabsorption, incoherent scattering, and coherent scattering in the energy range of this work are based on theoretical calculations (Scofield, 1973; Veigele, 1973; Hubbell et al., 1975; Chantler, 1995) and a semiempirical analysis (Henke et al., 1993). There are also a number of dedicated theoretical calculations of the cross sections for helium photoabsorption (Salpeter and Zaidi, 1962; Reilman and Manson, 1979; Hino et al., 1993; Kornberg and Miraglia, 1993; Andersson and Burgdörfer, 1994b; Pan and Kelly, 1995; Forrey et al., 1997; Yan et al., 1998; Kheifets and Bray, 1998; Johnson, 2000) and Compton scattering (Bergstrom et al., 1995; McGuire et al., 2000). The XCOM data base (Berger et al., 1999) uses photoabsorption data from Scofield (1973) and scattering data from Hubbell et al. (1975). Experimental data for the integral helium cross section in the keV regime exist only for X-ray attenuation (Azuma et al., 1995; Saloman et al., 1988), which is the sum of the absorption and scattering cross sections. Samson et al. (1994) reported a relative measurement of the Compton single ionization cross section.

We have measured the cross-section ratio of Compton scattering to photoabsorption in single ionization of helium between 7 and 16 keV. Two data points on this ratio at 4.5 and 5.5 keV obtained with a similar technique have recently been published by Morgan and Bartlett (1999). These ratios can be compared with ratios formed by theoretical calculations for Compton scattering and photoabsorption. In those cases where calculations refer to the total ionization cross section the experimental single-ionization ratios have to be modified to total ionization ratios by augmenting the single ionization ratio with $(1+R_C)/(1+R_P)$, using the experimental R_C and the asymptotic value of R_P from Section 2.2. The single ionization and total ionization ratios are very similar, because both R_C and R_P are $\sim 1.5\%$ in the region of interest. The total ionization results are plotted in Fig. 4a and shown with ratios from cross-section tabulations. The experimental ratios and the tabulations all show the same trend, however the logarithmic representation of Fig. 4a is too coarse to make quantitative comparisons. The experimental error bars in part (a) of this figure are smaller than the size of the symbols and two lines denoting the tabulations of Berger et al. (1999) and Veigele (1973) partly obscure each other. The experimental values of Morgan and Bartlett (1999), quoted without error limits, are seen to lie lower than all of the theoretical predictions.

A more quantitative comparison between experimental and theoretical Compton-to-photoabsorption ratios can be made using a χ^2-test. To this end we created a data base of published cross section data for single ionization or total ionization, Compton scattering and photoabsorption. In some cases we used cubic spline interpolations if theoretical results weren't available for the energies of our measurement. Ratios were formed for all possible combinations between Compton scattering and photoabsorption cross sections and compared to the experimental ratios at the respective energies using the χ^2-test. We found a very good match of theory and experiment for the combination of Hubbell et al. (1975) for Compton scattering and Yan et al. (1998) for photoabsorption. There were also other combinations that gave similarly good matches, but several combinations gave substantially worse agreement.

The cross section values of the favored combination was subsequently used to renormalize the experimental ratios into photoabsorption cross sections, i.e. normalizing the inverse of the ratio to Hubbell et al. (1975), or into Compton scattering cross sections, i.e. normalizing the ratio to Yan et al. (1998). The results of these two renormalizations are shown in Fig. 4b and 4c, respectively. We will use this as a consistency check of the various calculations for the two interactions. The photoabsorption cross section in Fig. 4b is plotted as $\sigma_P E^{3.5}$ in order to remove the rapid fall-off of the cross section and thus to show these results on a linear scale for better comparison. The data points by Morgan and Bartlett (1999), after the renormalization to

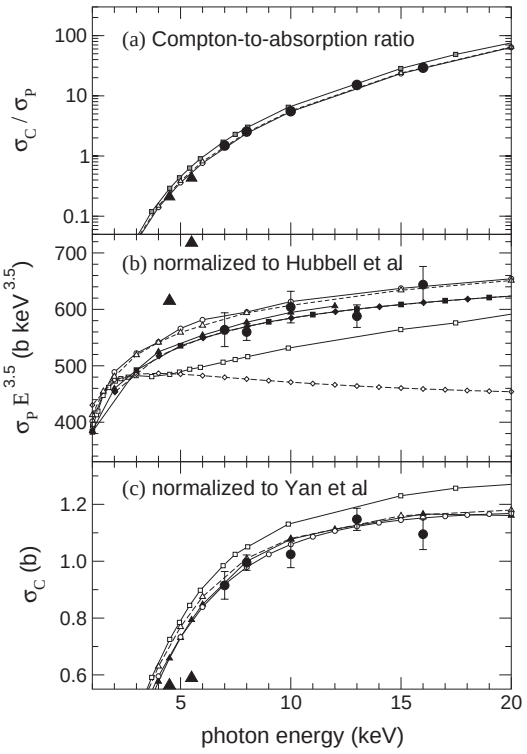

Fig. 4. The ratio of Compton scattering to photoabsorption in helium. Solid circles, this work; solid triangles, Morgan and Bartlett (1999). (a) Compton-to-photoabsorption ratio. Theories, from top to bottom: solid line with open squares, Henke et al. (1993); dashed line with open triangles, Veigele (1973); solid line with open circles, obscured, Berger et al. (1999). (b) Photoabsorption cross section multiplied by $E(\mathrm{keV})^{3.5}$. Experimental data normalized to Hubbell et al. (1975). Theories: solid line with small open circles, Scofield (1973); dashed line with small open triangles, Veigele (1973); solid line with small solid triangles, Hino et al. (1993); solid line with small solid squares, Yan et al. (1998); dashed line (obscured) with small solid diamonds, Johnson (2000); solid line with small open squares, Henke et al. (1993); dashed line with small open diamonds, Chantler (1995). (c) Compton scattering cross section. Solid-symbol experimental data normalized to Yan et al. (1998); Theories: solid line with small open squares, Henke et al. (1993); dashed line with small open triangles, Veigele (1973); solid line with small solid triangles, Bergstrom et al. (1995); solid line with small open circles, Hubbell et al. (1975).

photoabsorption cross sections in the same way, lie substantially outside of the various theoretical predictions.

We limit the discussion of the theoretical results to a few features found for different approaches. One independent check of the validity of a calculated photoabsorption cross section is to test the Thomas–Reiche–Kuhn sum rules, which are valid in nonrelativistic dipole approximation and are known to high accuracy from atomic structure calculations. It turns out that the high energy dependence of the cross section of Yan et al. (1998), which is favored by our measurements, gives a very good result for the $S(+2)$ sum rule in which the high energy part of the cross section is more heavily weighted. A recent reassessment of the helium sum rules can be found in Berkowitz (2002).

Another noteworthy feature seen in Fig. 4b is the close agreement between the nonrelativistic result of Yan et al. (1998) in dipole approximation with the results of the relativistic multipole independent particle approximation (IPA) calculation of Johnson (2000) evidencing the long-known cancellation of relativistic and multipole effects (Oh et al., 1976). The photoabsorption cross section of Scofield (1973) is also of the relativistic multipole IPA type. It lies about 5% higher than Johnson's results and this difference can be attributed to the omission of exchange. Applying the correction factor to account for exchange as listed in Scofield (1973) practically removes the difference between the two IPA calculations. The authors of the tabulation Berger et al. (1999) however stated that they get usually better agreement with experiment if the correction factor is omitted. We find that for helium the correction factor should definitely be applied in order to get an accurate measure of the cross section in the keV regime. The tabulated values of Veigele (1973), from a nonrelativistic Hartree–Fock calculation, are close to the uncorrected values of Scofield. The tabulations of Henke et al. (1993) and Chantler (1995) deviate by substantial amounts from the calculation favored by the experiment and by the sum-rule analysis.

It is an important question to ask for each calculation to what extent ionization-excitation and double ionization are included. It turns out that for calculations performed in the central-field or random-phase approximations, even though only the transition element between the initial and final ground states is evaluated, the result actually reflects total ionization (Cooper, 1996). To calculate accurate cross sections for specific final ionic states encountered in ionization-excitation and double ionization one must use highly correlated Hylleraas or configuration interaction (CI) wavefunctions for the initial state (Salpeter and Zaidi, 1962; Andersson and Burgdörfer, 1993; Kheifets and Bray, 1998; Yan et al., 1998). The total cross section is then the sum over all possible final state channels. The latter calculations give very reliable results for the total ionization cross section in the keV region. The result of the MBPT calculation of Hino et al. (1993) for single plus double ionization is higher than the favored photoabsorption cross section by the amount of double ionization. In both MBPT results (Hino et al., 1993; Pan and Kelly, 1995) the cross section for single ionization to the ionic ground state $He^+(1s)$ is very close to the favored result of total photoabsorption.

For completeness we show in Fig. 4c the renormalization of the experimental Compton-to-absorption ratio to Compton scattering cross sections. The favored results (Hubbell et al., 1975) are very close to those of Veigele (1973) and Bergstrom et al. (1995) in the region of our measurement. This is somewhat curious because the former two refer to incoherent scattering, which also includes nonionizing Raman scattering, and only the latter deals just with Compton scattering. We estimated the Raman contribution in the energy range of our experiment to decrease from about 5% at 7 keV to 1% at 16 keV. From our experimental results and the consistency check with photoabsorption we conclude that the values listed in Hubbell et al. (1975) for incoherent scattering are a good approximation of the cross section for Compton scattering.

On the basis of the analysis of our measurements of the Compton-to-photoabsorption ratio a consistent picture has emerged as to the absolute magnitudes of the photoabsorption and Compton scattering cross sections in the 7–16 keV energy region.

3. Nondipole photoelectron asymmetries

Atomic photoionization has long been studied as a fundamental process (Bethe and Salpeter, 1957) and for applications such as interpreting structure in the X-ray absorption spectra of materials (Stern, 1988). The development of synchrotron radiation sources of intense, tunable, polarized photon beams along with electron-spectrometer instrumentation enabled studies of the energy variations of partial photoionization cross sections and photoelectron angular distributions (Schmidt, 1992). This capability has been coupled with the development of theoretical methods to treat resonance, threshold, and many-electron interactions (Starace, 1982; Amusia, 1990) and produced detailed insight into atomic photoionization phenomena. The vast majority of such studies adopted the dipole approximation to the photon–electron interaction, because that approximation is adequate for studies of angle-integrated cross sections and of the dipole anisotropy of photoelectron angular distributions, with both quantities being sensitive to energy variations in the photoionization process. However, even early measurements of photoelectron angular distributions in the X-ray regime required treatments beyond the dipole approximation (Bethe and Salpeter, 1957). The early experimental and theoretical work are described by Jenkin (1981) in a review of the development of angle-resolved photoelectron spectroscopy. Before synchrotron radiation sources became readily available, soft X-ray lines below 2 keV were used to observe small enhancements of photoelectron intensities in the forward direction with respect to the X-ray beam (Krause, 1969; Wuilleumier and Krause, 1974). Those asymmetries were accounted for qualitatively by retardation correction factors (Cooper and Manson, 1969) that are based on high-energy-limit models such as the Born approximation (Bethe and Salpeter, 1957) and predict nondipole asymmetries to vary as v/c, i.e., for angular distributions to be skewed increasingly "forward" with respect to the photon propagation vector as the photoelectron velocity v increases. Modern theories calculate photoionization amplitudes in screened potentials and obtain much more interesting variations of nondipole asymmetries with energy, especially close to ionization thresholds and in energy regions where dipole and quadrupole photoionization amplitudes strongly vary (Tseng et al., 1978; Bechler and Pratt, 1989, 1990; Scofield, 1990; Cooper, 1993; Derevianko et al., 1999; Dolmatov and Manson, 1999; Johnson and Cheng, 2001; Amusia et al., 2001). Combining modern theoretical treatments with experiments using tunable synchrotron radiation, the study of nondipole asymmetries has developed into a tool for the investigation of photoionization dynamics.

The first experiments using synchrotron radiation to measure nondipole asymmetries studied rare-gas atoms over broad energy ranges and compared with theory (Krässig et al., 1995; Jung et al., 1996; Hemmers et al., 1997). Soon after, nondipole asymmetries were measured in solids and understood using the formulation developed for free atoms (Fisher et al., 1998; Jackson et al., 2000). Theoretical treatments have also been developed specifically for solid state experiments (Nefedov and Nefedova, 2000; Vartanyants and Zegenhagen, 2000). Many-electron interactions were observed in nondipole asymmetries by measurements of autoionizing quadrupole and dipole resonances in low-energy valence-shell photoionization of atomic Cd (Martin et al., 1998) and He (Krässig et al., 2002; Kanter et al., 2003), and calculational studies were reported for Ne and Ar (Dolmatov and Manson, 1999). The nondipole asymmetry parameter of Xe 5s photoelectrons was calculated and measured over the $\approx$26–200 eV photon energy range and demonstrates one-electron and many-electron effects, including interchannel coupling among quadrupole photoionization channels (Amusia et al., 2001; Johnson and Cheng, 2001; Ricz et al., 2003; Hemmers et al., 2003). The nondipole asymmetry measured for K-shell photoelectrons of molecular N_2 greatly exceeds the asymmetry calculated for atomic N, an effect that was explained by treating nondipole interactions in molecular photoionization (Hemmers et al., 2001; Langhoff et al., 2001). An experimental and theoretical study of K-shell photoelectrons from fixed-in-space N_2 was also reported (Guillemin et al., 2002). Some of the results obtained on atoms and molecules at lower energies are reviewed elsewhere in this volume (Lindle et al., 2004). The discussion here is limited to a

description of the experimental methods used and results obtained for the inner shells of rare gas atoms using X rays in the range ≈2–22 keV (Krässig et al., 1995, 2003; Jung et al., 1996).

The nonrelativistic expression for the photoionization matrix element between the bound state $|i\rangle$ and continuum state $|f\rangle$ is

$$M_{if} = \langle f| \exp(i\boldsymbol{k}\cdot\boldsymbol{r})\boldsymbol{\varepsilon}\cdot\boldsymbol{p}|i\rangle, \quad (1)$$

where $\boldsymbol{k}$ is the photon propagation vector, $\boldsymbol{r}$ is the electron position vector, $\boldsymbol{\varepsilon}$ is the linear-polarization vector of the photon, and $\boldsymbol{p}$ is the electron momentum operator. The differential cross section is proportional to $|M_{if}|^2$ and, in general, depends on the angles between the photoelectron momentum vector and both $\boldsymbol{\varepsilon}$ and $\boldsymbol{k}$. Leading correction terms to the dipole approximation can be included by adopting the "retardation expansion" of the exponential factor in Eq. (1):

$$\exp(i\boldsymbol{k}\cdot\boldsymbol{r}) \approx 1 + i\boldsymbol{k}\cdot\boldsymbol{r} - \frac{1}{2}(\boldsymbol{k}\cdot\boldsymbol{r})^2 + \cdots. \quad (2)$$

The retardation expansion (Bechler and Pratt, 1989, 1990) is not the same as the multipole expansion (Peshkin, 1970). Treating a finite number of terms in Eq. (2) includes a finite number of multipoles within the long-wavelength limit ($k \to 0$). Keeping only the leading term, $\exp(i\boldsymbol{k}\cdot\boldsymbol{r}) \approx 1$, is the "nonretarded dipole approximation" and treats the photon–electron interaction as an electric-dipole (E1) process in the long-wavelength limit. Since there is no dependence on the direction of $\boldsymbol{k}$ in the dipole approximation, calculated angular distributions are symmetric with respect to reversal of $\boldsymbol{k}$.

The "first retardation correction" consists in keeping the second term in the expansion, $\exp(i\boldsymbol{k}\cdot\boldsymbol{r}) \approx 1 + i\boldsymbol{k}\cdot\boldsymbol{r}$, which introduces long-wavelength limits of electric-quadrupole (E2) and magnetic-dipole (M1) interactions. Retaining terms to order kr in calculations of $|M_{if}|^2$ then includes E1–E2 and E1–M1 cross terms, i.e., interference between E1 photoionization amplitudes and those for E2 and M1 interactions, but excludes E2–E2, M1–M1, and E2–M1 terms that are of order $(kr)^2$. The E1–E2 and E1–M1 cross terms have odd parity and produce asymmetries in angular distributions with respect to reversal of the direction of $\boldsymbol{k}$. For photoionization of randomly oriented atoms by a linearly polarized photon beam and including terms up to first order in kr, the differential cross section can be expressed as (Cooper, 1993)

$$\frac{d\sigma}{d\Omega}(\theta,\phi) = \frac{\sigma}{4\pi}\{1 + \beta P_2(\cos\theta) + (\delta + \gamma\cos^2\theta)\sin\theta\cos\phi\}, \quad (3)$$

where σ is the angle-integrated cross section, β is the dipole anisotropy parameter, $P_2(\cos\theta) = (3\cos^2\theta - 1)/2$ is the second Legendre polynomial, and δ and γ parameterize the nondipole asymmetries resulting from E1–E2 and E1–M1 cross terms. The coordinate axes for Eq. (3) are shown in Fig. 5, with the positive x axis along the direction of $\boldsymbol{k}$, the z axis along the linear polarization vector $\boldsymbol{\varepsilon}$, and θ and ϕ are the polar and azimuthal angles of the photoelectron momentum vector.

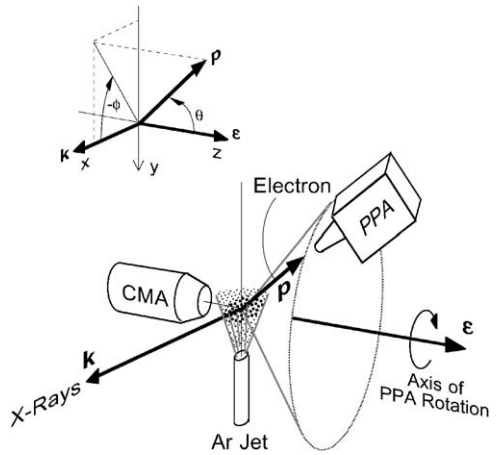

Fig. 5. Instrumentation used to measure nondipole asymmetries of photoelectron angular distributions. The polar angles of the photoelectron momentum vector $\boldsymbol{p}$ are indicated with respect to coordinate axes defined by the propagation vector $\boldsymbol{k}$ and polarization vector $\boldsymbol{\varepsilon}$ of the X-ray beam.

3.1. Experimental geometries

Given the form of Eq. (3), Shaw et al. (1996) discussed various experimental approaches to measuring β, δ and γ. They also considered modifications to Eq. (3) in practical cases of partially linearly-polarized photon beams and small misalignments of the experimental geometry with the $\boldsymbol{k}$ and $\boldsymbol{\varepsilon}$ vectors of the photon beam. Those experimental issues were accounted for in our measurements of Ar 1s and Kr 2s and 2p subshells (Krässig et al., 1995; Jung et al., 1996) made using 2–5 keV X rays with the instrumental setup sketched in Fig. 5. A parallel-plate electron analyzer (PPA) was mounted on a rotation stage at the magic polar angle $\theta_m = 54.7°$, where $P_2(\cos\theta_m) = 0$, but could be rotated over the full $\phi = 0 - 360°$ range of the azimuthal angle. With this measurement geometry, the dependence on β is eliminated from Eq. (3), and the variation of the photoelectron intensity with ϕ depends on the nondipole asymmetry parameters:

$$I(\theta_m,\phi) = I_0[1 + (2/27)^{1/2}(\gamma + 3\delta)\cos\phi], \quad (4)$$

where I_0 is proportional to the product of the angle-integrated cross section σ, the photon flux, and target gas density. Alignment apertures ensured that the rotation axis was perpendicular to $\boldsymbol{k}$ to avoid introducing a systematic forward–backward asymmetry

(Shaw et al., 1996). A cylindrical-mirror electron analyzer (CMA) was positioned opposite the PPA to provide a normalization signal for electron intensities measured with the PPA at different angles. The normalization signal accounted for variations in the X-ray beam flux and overlap of the X-ray beam and gas jet. Photoelectron intensities were measured at 15° angular steps, as shown in Fig. 6 for Ar 1s at 2000 eV kinetic energy. The data were corrected for an instrumental asymmetry of $\approx \pm 10\%$ due to variation of the observed interaction volume with ϕ. The instrumental asymmetry was determined from measurements of the intensities of Auger electrons vs. ϕ, since Auger electrons have zero first-order nondipole asymmetries in the limit of a two-step model of the vacancy-decay process (Kabachnik and Sazhina, 1996) and K-LL Augers have $\beta = 0$. Qualitatively, the data in Fig. 6 show that the Ar 1s angular distribution at 2000 eV is enhanced in the "forward" direction ($\phi \approx 0°$) compared with "backward" ($\phi \approx 180°$). To determine $\gamma + 3\delta$ from the data, Eqs. (3) and (4) were modified to account for $\approx 95\%$ degree of linear polarization of the X-ray beam and $\approx 1°$ misalignment of the PPA rotation axis with the polarization ellipse. The curve through the data in Fig. 6 is the result of a fit that accounts for those instrumental factors and yields the experimental result for $\gamma + 3\delta$. Since $\delta \approx 0$ for an *ns* subshell, even in a relativistic model (Derevianko et al., 1999), our measurements determine γ in this case.

Before discussing the results obtained with the first setup, we briefly describe an improved instrument that was used for measurements of Kr 1s using ≈ 14–22 keV X rays (Krässig et al., 2003). Four PPAs are mounted on a rotation stage at 54.7° with respect to the rotation axis, and the rotation axis is perpendicular to both $\boldsymbol{k}$ and $\boldsymbol{\varepsilon}$ of the X-ray beam (see Fig. 7). Alignment apertures ensure a high degree of perpendicularity between $\boldsymbol{k}$ and the rotation axis. This is a versatile measurement geometry that can be used to determine separate values of β, δ, and γ if the degree of linear polarization is known (Shaw et al., 1996). However, for measurements of $\gamma + 3\delta$, we take advantage of a symmetry property of photoelectron angular distributions that was explained by Peshkin (1996). With polar angles (θ', ϕ') referenced to the photon $\boldsymbol{k}$ vector, the average of photoelectron intensities measured at the same θ' but at ϕ' angles differing by 90° is independent of the polarization state of the photon beam and equal to that for an unpolarized beam at θ'. To make use of this symmetry property, along with eliminating the dependence on β, the rotation stage is positioned with the PPAs along the diagonals of a cube whose faces are normal to the coordinate axes. These positions are "magic" with respect to all three axes, i.e., the direction cosines are all $\pm 1/\sqrt{3}$. The PPAs numbered 1 and 4 in Fig. 7 are both at $\theta' = 54.7°$, but their azimuthal angles differ by 90°. Similarly, the PPAs numbered 2 and 3 are at $\theta' = 125.3°$, but their azimuthal angles differ by 90°. It follows that the nondipole

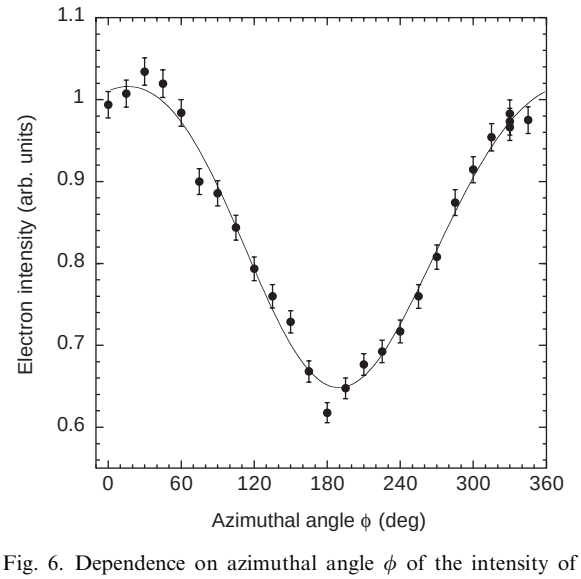

Fig. 6. Dependence on azimuthal angle ϕ of the intensity of 2000 eV Ar 1s photoelectrons at fixed polar angle $\theta = 54.7°$ after correction for the instrumental asymmetry. The solid curve is a fit to the data used to determine the nondipole asymmetry parameter γ and accounts for the degree of linear polarization of the X-ray beam and tilt of the polarization ellipse.

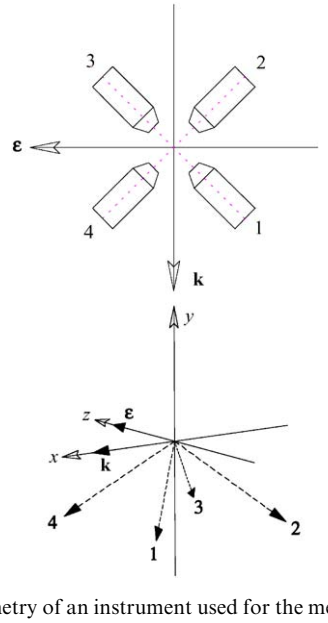

Fig. 7. Geometry of an instrument used for the measurement of nondipole asymmetries of photoelectron angular distributions. Four electron analyzers, labeled 1–4, are positioned as indicated with respect to the propagation vector $\boldsymbol{k}$ and polarization vector $\boldsymbol{\varepsilon}$ of the photon beam. The bottom figure shows a trimetric view and the top figure shows a projection in the $\boldsymbol{\varepsilon}-\boldsymbol{k}$ plane.

asymmetry can be determined, independent of the polarization properties of the X-ray beam and of β, from the following combination of photoelectron intensities:

$$A = \frac{I_1 - I_2 - I_3 + I_4}{I_1 + I_2 + I_3 + I_4}. \quad (5)$$

The rotation stage is rotated to measure photoelectron intensities with each PPA at each of the four positions, and the results are averaged. Averaging accounts for variations in the PPA collection efficiencies and reduces systematic errors. The photoelectron intensities were normalized to the intensity of Kr K X-ray fluorescence measured by a NaI scintillation detector to account for variations in X-ray beam flux and overlap with the gas jet. The four PPA positions view equivalent projections of the interaction volume, and the instrumental asymmetry was reduced to $\pm 3\%$ based on Auger electron measurements. The experimental asymmetry parameter A can be compared with the first-order nondipole corrections expressed in Eq. (3) by $A = (27)^{-1/2}(\gamma + 3\delta)$. Comparison can also be made with higher-order corrections, e.g., the second-order expression that results from treating the first three terms of Eq. (2) (Derevianko et al., 1999; Krässig et al., 2003).

3.2. Nondipole asymmetries of argon and krypton

Our measured γ parameters for Ar 1s and Kr 2s agree well within experimental uncertainties with relativistic independent-particle-approximation (IPA) (Derevianko et al., 1999) and nonrelativistic IPA calculations (Bechler and Pratt, 1989, 1990; Cooper, 1993) as shown in Figs. 8 and 9. The γ parameter can be negative as well as positive, meaning that the angular distribution can be tilted backwards as well as forwards with respect to the photon $\boldsymbol{k}$ vector. The distinct energy variations of γ for Ar 1s and Kr 2s reflect its dependence on El and E2 photoionization amplitudes. To see this, it is useful to consider a model in which first-order retardation corrections are treated within the nonrelativistic IPA (Bechler and Pratt, 1989, 1990; Cooper, 1993). For the case of an atomic ns subshell, there are only two continuum waves to consider, $n\mathrm{s} \rightarrow \varepsilon\mathrm{p}$ and $n\mathrm{s} \rightarrow \varepsilon\mathrm{d}$, produced by El and E2 interactions, respectively. This simplifies the angular distribution in Eq. (3) to the form with $\beta = 2$, $\delta = 0$, and the nondipole asymmetry is characterized by γ. The γ parameter is determined by interference between the p-wave and d-wave amplitudes and can be expressed in atomic units as (Cooper, 1993)

$$\gamma = 3\alpha\omega \frac{Q}{D} \cos(\delta_2 - \delta_1), \quad (6)$$

where α is the fine-structure constant, ω is the photon energy, D, Q are the radial dipole and quadrupole matrix elements, and $\delta_{1,2}$ are the asymptotic phase shifts.

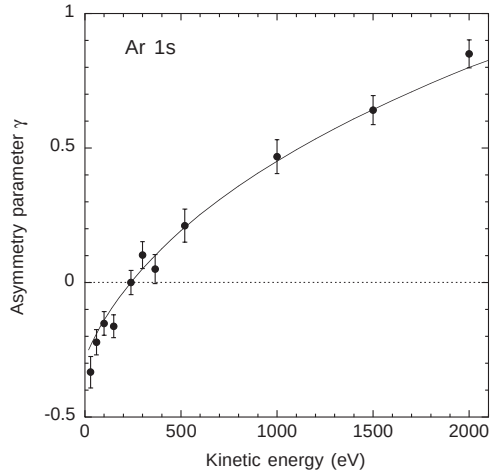

Fig. 8. Measurements and independent-particle-approximation calculations (Derevianko et al., 1999) of the Ar 1s nondipole asymmetry parameter.

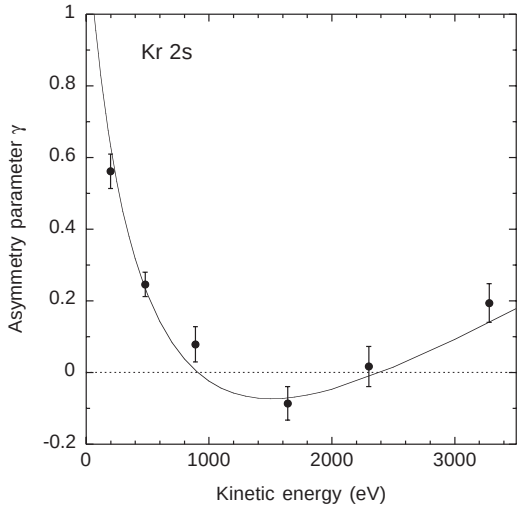

Fig. 9. Measurements and independent-particle-approximation calculations (Derevianko et al., 1999) of the Kr 2s nondipole asymmetry parameter.

The variations of γ with energy can thus be traced to variations of the magnitudes and phases of the photoionization amplitudes. Bechler and Pratt (1989, 1990) explained that the threshold values and positive and negative excursions of γ with energy of 1s and 2s subshells result from the signs and magnitudes of Q, D, and $\cos(\delta_2 - \delta_1)$. Furthermore, the signs and number of zeroes of Q and D are sensitive to details of the bound- and continuum-state radial functions, such as the presence of a node in the 2s function. For $n\ell$ ($\ell > 0$) subshells, two partial waves are produced by the E1 interaction and three are produced by the E2 interaction. Consequently, both γ and δ are nonzero, and their

formulation is more complicated than for *n*s subshells. Our measurements of $\gamma+3\delta$ for Kr 2p photoelectrons agree well with nonrelativistic IPA calculations (Jung et al., 1996).

In Fig. 10, Kr 1s asymmetries are compared with nonrelativistic IPA calculations and with the point-Coulomb model that predicts $\gamma=12(v/c)$ (Bechler and Pratt, 1989; Krässig et al., 2003). The point-Coulomb model adopts hydrogenic wavefunctions, neglecting screening by other electrons, and results in the retardation correction vanishing at threshold and increasing monotonically with energy. This model breaks down for Kr 1s as the energy is lowered toward threshold. As discussed fully by Bechler and Pratt (1989), Krässig et al. (2003), screening affects both the normalizations and asymptotic phase shifts of the p- and d-wave continuum functions. The rapid variation of γ calculated in the $\approx$1–10 eV region is attributed to an IPA shape resonance in the d-wave channel.

In summary, the variations of nondipole asymmetries of atomic inner shells within a few keV of threshold depend on details of bound and continuum state wavefunctions through the magnitudes and phases of dipole and nondipole photoionization amplitudes. Comparison with existing measurements indicates that these quantities are well described by IPA calculations. At sufficiently high energies, the screened IPA calculations give increasingly forward-directed angular distributions in rough agreement with the point-Coulomb model (Bechler and Pratt, 1989, 1990).

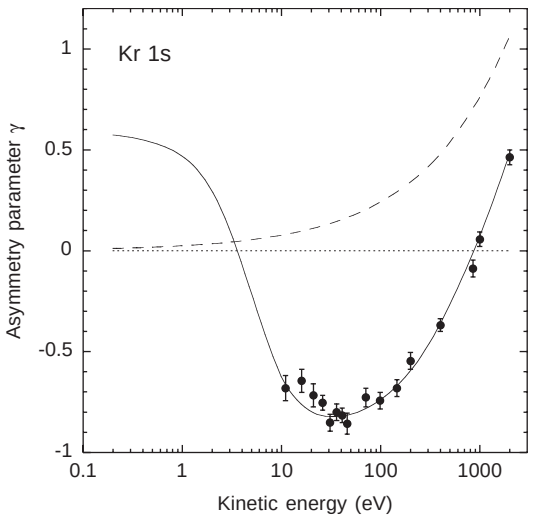

Fig. 10. Measurements and calculations (Bechler and Pratt, 1989) of the Kr 1s nondipole asymmetry parameter. The dashed curve is the $12(v/c)$ prediction of the point-Coulomb model, and the solid curve includes screening within the independent-particle approximation.

4. Production and decay of double K vacancies

The formation and decay of atoms with empty K shells was first considered by Heisenberg (1925) during the early development of quantum mechanics. It then became an important subject in nuclear physics because of the predictions of Migdal (1941) and Feinberg (1941) of the production of such atomic systems in nuclear α and β decay processes. For $Z>40$, when K-fluorescence yields become large, the predominant decay of such states is through the sequential emission of two K X rays. In 1953, Charpak (1953) first observed such X-ray cascades following the electron capture (EC) decay of ^{55}Fe by coincident detection of the X rays in a pair of proportional counters. Since that time, many workers have investigated the production and decay of such hollow atoms in α,β, electron capture, and internal conversion (IT) decays of radioactive nuclei (Freedman, 1974).

Briand et al. (1971) were the first to point out the large energy shifts (from the normal diagram lines) of the $K^{-2}\rightarrow K^{-1}L^{-1}$ transitions which they termed *hypersatellites* in contrast to the more common satellite transitions when there are multiple vacancies in the upper levels of the initial state. Using radioactive sources, several atomic structure aspects of such decays have been investigated including the suppression of the $K\alpha_1$ transition (Briand et al., 1976), relativistic effects (Mukoyama and Shimizu, 1975), and the importance of electron–electron correlations (Briand et al., 1981).

While such work has been quite illuminating, it has also been somewhat limited because of the necessity of using radioactive sources. Because of the change in nuclear charge in α, β, and EC decays, shakeup and shake-off processes dominate the production of double K vacancies with such sources. In contrast, in IT decays, the Coulomb field of the nucleus remains essentially unchanged and, especially near threshold, there can be substantial contributions from correlated electron motions. Unfortunately, with IT, the exciting photon (in this case virtual) is of *fixed* energy. Previous attempts to study such systems by photoionization using X-ray tubes have been similarly hampered (Keski-Rahkonen et al., 1977; Ahopelto et al., 1979) because of the limited photon flux and tunability. In recent years, several groups have exploited modern synchrotron radiation sources to probe the formation and decay of such double K-vacancy states with tunable X-rays and we will briefly summarize that work here.

4.1. Theoretical background

It has long been recognized that the double excitation and ionization of He-like systems by photoabsorption provides a precise test of electron correlations and dynamics in atoms. Experimentally however, this has

been difficult to achieve in all but the lightest systems ($Z \leqslant 3$) (Lubell, 1995). Because double ionization proceeds through the Z-independent e–e interaction, the effect of electron–electron correlations has in fact been found to be *constant* with increasing Z (Briand et al., 1981) and consequently more challenging to treat in high-Z systems where relativistic effects simultaneously become important (Berry et al., 1993). Because of the relative isolation of the K-shell electrons from the outer shells in heavy atoms, the double-K ionization of a heavy atom, producing a hollow atom, is comparable to the double ionization of the same heliumlike system, stripped of the outer shell electrons.

In many-body perturbation theory there are three terms which contribute in first order: so-called "two step one" (TS1), shake-off (SO), and ground state correlations (GSC) as shown in Fig. 11. In the latter (GSC), electronic interaction *precedes* photoabsorption and thus is sensitive to electron correlations in the initial state. For the other two terms, the electronic interaction is after photoabsorption and thus they are sensitive to correlations in the intermediate state with a K-vacancy. In TS1, the final interaction is between an *electron* and the other electron, essentially representing electron–electron scattering. For shake-off, the final interaction is between the *hole* and the remaining electron, and thus represents the relaxation of the vacancy excitation. The relative contributions of these terms has been shown to be gauge-dependent (Hino et al., 1993). As noted earlier (see Section 2.2), in the "sudden approximation" the SO and GSC are lumped together as shake processes while the dynamical scattering process described by TS1 is excluded. As was recently pointed out in the case of He double-ionization (Schneider et al., 2002), the scattering and shake terms can be isolated from their very different energy dependences. Because of the energy dependence of electron–electron scattering, TS1 is most prominent at lower energies and is strongly energy dependent. At higher energies, double photoionization of the K-shell has been discussed extensively in terms of shake processes where a fast photoelectron leaves with most of the available energy and then as the core-excited atom relaxes the second electron is shaken up/off leading to the concept of an energy-independent asymptotic limit of the ratio between double and single ionization (Åberg, 1970).

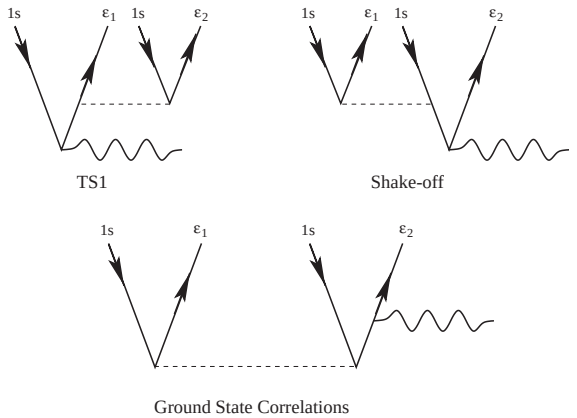

Fig. 11. Feynman diagrams showing the three first-order terms contributing to double-K photoionization: "Two-step-one", shake-off, and ground state correlations.

4.2. Experimental methods

Experimentally, the signal for detecting the presence of double K-vacancy states is a hypersatellite transition when the double-vacancy state decays. For low Z ($\lesssim 20$), when fluorescence yields are low, the best method has been high resolution Auger spectroscopy. As Z (and the fluorescence yield) increases, high-resolution X-ray spectroscopy is preferable. As we will demonstrate below, this becomes problematic for very high Z and, in that case, coincidence techniques are required. We will discuss each of these methods in more detail.

In the case of neon ($Z = 10$), the fluorescence yield of double-K-hole decay is predicted to be only 0.0247 (Chen, 1991). Furthermore, the Dirac–Fock predicted hypersatellite energy shift (~ 65 eV) of the KK-KLL Auger electrons (Chen, 1991) is appreciable compared to the 0.27(2) eV natural width of the single vacancy diagram line. Thus, with only moderate electron energy resolution, it is possible to separate the hypersatellite emission from the diagram lines. This was demonstrated recently in our experiment at APS where we observed the double K-shell photoionization of neon by measuring the KK-KLL Auger electron spectrum with high resolution (Southworth et al., 2003). An example of such a spectrum is shown in Fig. 12. From such data, the ratio (P_{KK}) of double- to single-K photoionization was found to be 0.32(4)%.

With increasing atomic number Z, the hypersatellite shift increases roughly as Z^2, while the fluorescence yields grow even faster (Bambynek et al., 1972). Thus for $Z \gtrsim 20$, high resolution X-ray spectroscopy becomes practical allowing work with solid targets. This was recently demonstrated by Deutsch and collaborators in a beautiful series of experiments at the NSLS at Brookhaven National Laboratory (Diamant et al., 2000a, b). Using a curved crystal spectrometer, they measured the Cu $K^h\alpha_{1,2}$ hypersatellite emission spectrum following double-K photoionization by 18–25 keV photons. Similar measurements have since been reported for Ca, Ti, and V ($Z = 20$, 22, 23) with photons in the range of 8–35 keV from SPring-8 (Oura et al., 2002).

This method is very appropriate for such mid-Z elements, but becomes problematic for heavier atoms. This is because asymptotically, the ratio of double/single K-photoionization is expected to fall off with $1/Z^2$ as is

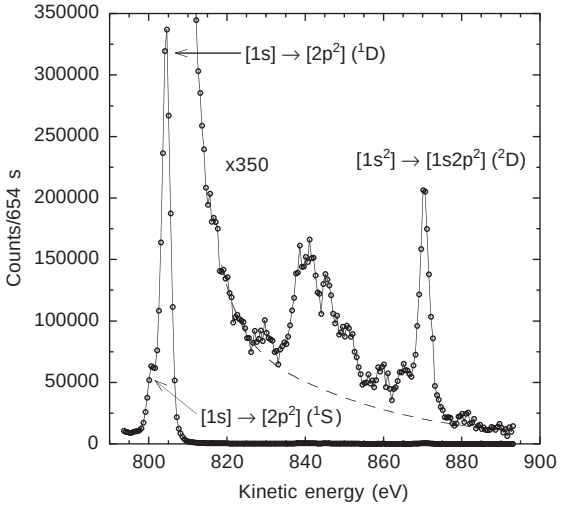

Fig. 12. Auger electron spectrum of Ne observed following photoionization by 5 keV photons. The normal diagram lines produced by the decay of single-K vacancies are in the lower energy region while the hypersatellite transitions (magnified) lie on the high-energy tail of the more intense diagram lines.

observed for shake-off. On the other hand, the natural line width of the diagram line grows with Z^4 while the hypersatellite energy shift from the diagram line only increases roughly as Z^2 (Chen et al., 1982). The net result is that with increasing Z, the hypersatellite/diagram tail intensity ratio is numerically found to fall off as $\sim 1/Z^3$ and thus the diagram line becomes the limiting background for such singles measurements, regardless of improvements in resolution or angular acceptance. Thus, to study double-K photoionization in the heaviest atoms, coincidence techniques are required to isolate the hypersatellite transitions from the far more probable diagram lines.

In 1999, our group first observed the double-ionization of the K shell of a heavy atom (molybdenum, $Z=42$) with synchroton radiation (Kanter et al., 1999). The experiment was performed on the BESSRC 12BM bending magnet beam-line at the APS. We used the method of satellite-hypersatellite coincidences, pioneered by Briand et al. (1971), with 50-keV incident photons. This energy is close to that corresponding to the predicted maximum (~ 53 keV) in the double photoionization cross section for He-like Mo (Kornberg and Miraglia, 1994).

The target consisted of a 25-μg/cm^2 film of natural molybdenum deposited on a 5-μg/cm^2 carbon foil and oriented with the surface at an angle of 30° with respect to the incident beam. Two Si(Li) detectors faced each other and were normal to the beam, lying in the same plane as the beam polarization and the target normal. With this geometry, Compton and Rayleigh scattering were suppressed. Standard coincidence electronics recorded the energies deposited in each detector and the time difference between the detectors.

The region of the energy spectrum in each detector corresponding to K X rays is shown in Fig. 13 for those X rays detected in coincidence with K X rays in the other detector. The open squares in each spectrum correspond to "prompt" coincidences. The "delayed" accidental coincidences are shown as filled triangles (connected by solid lines). The main features in this region of the spectrum are the Kα and Kβ normal diagram lines in Mo at 17.5 and 19.6 keV respectively. The prompt spectra show a clear excess on the high-energy sides of each peak corresponding to the hypersatellite transitions which, because of the reduced screening in the hollow atom, are systematically shifted up in energy. From these measurements, the ratio P_{KK} was determined to be $3.4(6)\times 10^{-4}$ for 50 keV incident photon energy.

4.3. Hollow silver

In an effort to experimentally separate the dynamical scattering and shake terms in a heavy atomic system, we recently measured double K ionization of silver ($Z=47$) for several energies from threshold to the expected maximum (~ 100 keV) using the coincidence method at the APS (Kanter et al., 2004). A sample of the data is shown in Fig. 14 for the case of 90 keV incident photon

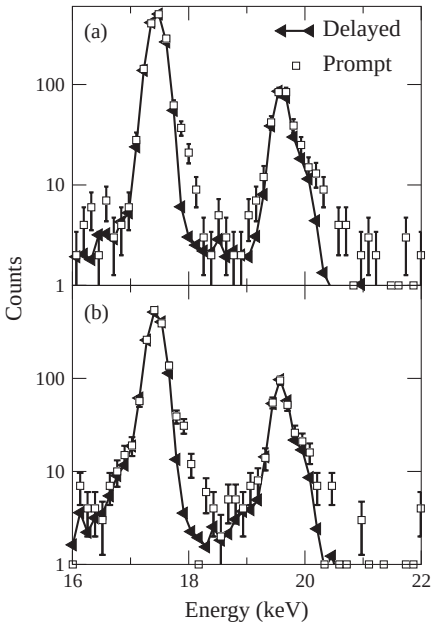

Fig. 13. Energy spectra in each detector for coincidences with Mo Kα,β X-rays in the other detector. Spectrum for detector "1" is in (a) while that for "2" is in (b). Incident photon energy was 50 keV on a thin Mo target. Data points (open squares) are for prompt coincidences while the filled triangles connected with the solid line correspond to delayed coincidences.

energy. Plotted are the energy spectra in each of the two detectors in the region of the K X rays for both prompt and delayed coincidences. The hypersatellites shifts are apparent in the prompt and absent in the random (delayed) spectra. We chose to study silver because of extensive measurements which have been previously carried out using the electron capture (EC) decay of ^{109}Cd in a radioactive source (Ko et al., 1998) producing hollowed ^{109}Ag. Because one of the electrons is absorbed in the nucleus, there is only a single free electron in the final state, and thus double K-ionization proceeds by a pure shake-off process. Hence, the asymptotic limit is determined independently by the radioactive source measurements.

The results are shown in Fig. 15 where in addition to our photoionization data (open circles) we have included the EC data of Ko et al. (1998) for the asymptotic limit. The solid line shows a best fit using the Thomas model (Thomas, 1984). This model, which has been used in the past to describe shake processes near threshold (Diamant et al., 2000b), uses time-dependent perturbation theory and produces a simple expression for the energy dependence which depends only on the radius and

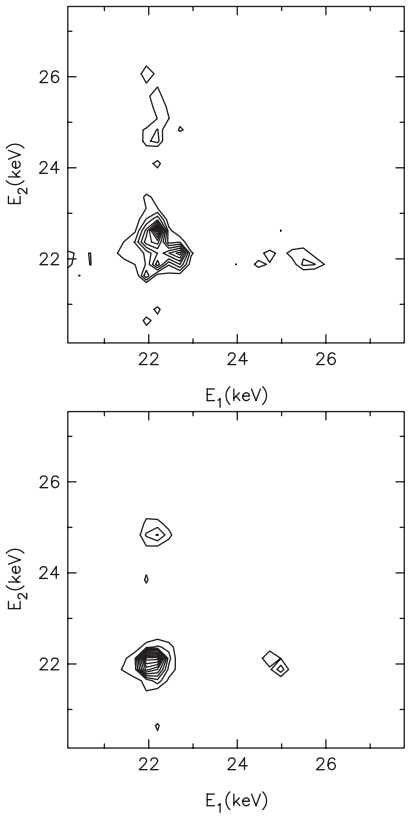

Fig. 14. Prompt (top) and delayed (bottom) coincidence energy spectra in the K X-ray region for double-K photoionization of Ag by 90 keV photons.

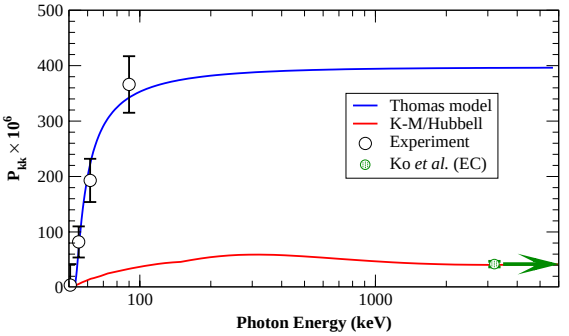

Fig. 15. The ratio of double to single K-ionization of silver as a function of photon energy. See text for explanations of the curves.

binding energy of the shaken electron. Because it completely neglects the strong energy dependence of the TS1 term near threshold, it simply predicts a monotonic rise to the asymptotic limit. However, in order to best-fit our photoionization data, the predicted asymptote is an order of magnitude higher than the EC result.

A better approximation of the results can be obtained by using the scaling law given by Kornberg and Miraglia (1994) for double-ionization of He-like ions and dividing by the single ionization cross section (Berger et al., 1999) shown as the dashed line in Fig. 15. It is evident that such a model is qualitatively much closer to the trend of the data, showing the predicted peak in the ratio and then declining to the asymptotic limit.

Because of the dominance of the TS1 term in the region of the broad maximum, it is instructive to plot the trend of P_{KK} in the peak region with Z as we suggested a few years ago (Kanter et al., 1999). Combining all of the available data, including our measurements on Ne, Mo, and Ag, we show that result in Fig. 16. We also show in Fig. 16 the earlier photoionization results (Ahopelto et al., 1979) in lighter atoms ($22 \leqslant Z \leqslant 28$). Those measurements were also carried out somewhat above threshold but well below the asymptotic regime.

Shake processes lead to a $1/Z^2$ fall-off in the double-K ionization probability (Levinger, 1953) and that is a predominant characteristic of all of the Z-scaling laws suggested for He-like ions. For comparison, we show in Fig. 16 one of those scaling laws (Forrey et al., 1995). That scaling law shows excellent agreement with the asymptotic ratios measured in He by Spielberger et al. (1995) and by the EC measurement in Ag (Ko et al., 1998). In contrast, those measurements in the peak region, besides being obviously systematically higher, also fall off significantly slower than the $1/Z^2$ dependence of shake-off. Surprisingly, all of the newer data show good agreement with the somewhat weaker $1/Z^{1.61}$ dependence which we reported earlier (Kanter et al., 1999).

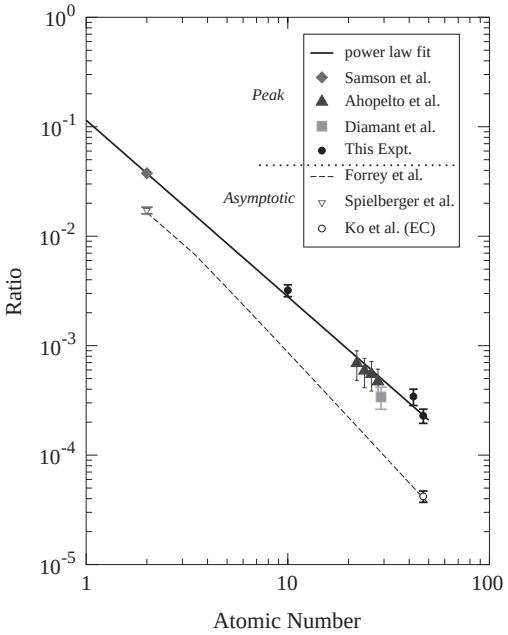

Fig. 16. The ratio of double to single K-ionization as a function of atomic number. The solid symbols are used for experiments carried out in the region of the predicted peak in the double ionization cross section while the open symbols are used for measurements of the ratio and the corresponding theoretical prediction (dashed curve) for the asymptotic energy limit. Also shown (solid line) is our $1/Z^{1.61}$ power-law fit.

This work has demonstrated that it is now possible, with modern 3rd-generation synchrotron sources, to explore the energy-dependence of double K-ionization in heavy atoms. Although this problem has been studied extensively in He, little attention has as yet been paid to heavier systems. In particular, the difficulties of simultaneously treating electron–electron correlations and relativity should pose an intriguing challenge.

5. Two photon decay of K vacancies in neutral atoms

The simultaneous emission of two photons is a rare decay mode for a K vacancy of an atom. Freund (1973) estimated the rate in Cu to be $\sim 10^{-6}$ of the one-photon decay rate. Although the sum of the energies of the two photons is equal to the transition energy, the energies of the individual photons vary continuously so this processes contributes to the continuum radiation on the low energy side of the characteristic X-ray lines. Two-photon decay is important from a theoretical standpoint as it provides a unique way of testing atomic structure calculations. Typical measurements provide information on decay rates differential in the opening angle distribution and the energies of the individual photons. Together these characteristics provide a wealth of information to test the details of the calculations.

The most important two-photon transitions involving an initial K hole are $ns \rightarrow 1s$ and $nd \rightarrow 1s$, involving the emission of two electric dipole photons (2E1). The theory of two-photon decay of the H-like $2s \rightarrow 1s$ transition in one-electron ions has been studied extensively. Parpia and Johnson (1982), and Goldman and Drake (1981) have completed fully relativistic calculations. Also, $nd \rightarrow 1s$ decays in H-like ions have been calculated by Florescu, Tung and their collaborators (Florescu et al., 1987; Tung et al., 1984; Florescu, 1984). These calculations provide predictions for all values of the nuclear charge Z. For K-vacancies in neutral atoms, calculations have been done for only a few special cases. Nonrelativistic self-consistent-field calculations exist for Mo (Bannett and Freund, 1982, 1984) and Xe (Wu and Li, 1988), and relativistic self-consistent-field calculations have been done for Mo, Ag, and Xe by Tong et al. (1990) and by Mu and Crasemann (1988).

5.1. Experimental observations of inner-shell two photon decay

Bannett and Freund (1984) made the first observation of two-photon decay of a K-vacancy in a heavy atom. They observed both the $2s \rightarrow 1s$ and the $3d \rightarrow 1s$ transitions following photoionization of Mo ($Z = 42$). Ilakovac and coworkers studied two-photon decay using radioactive sources in which the K-vacancies were produced via electron capture by the nucleus. They observed back-to-back two-photon decays for the $2s \rightarrow 1s$, $3s \rightarrow 1s$, $3d \rightarrow 1s$ and for the (unresolved) $4s \rightarrow 1s$, $4d \rightarrow 1s$ transitions in xenon ($Z = 54$), silver ($Z = 47$) and hafnium ($Z = 72$) (Ilakovac et al., 1986, 1991, 1992). They established the existence of all of these decay modes and verified the shapes of the continuum radiation including the resonance effect in the $3d \rightarrow 1s$ transitions (Ilakovac et al., 1992). In another experiment with a radioactive source, Schäffer and collaborators (Schäffer, 1999; Mokler and Dunford, 2001; Mokler et al., 2002) observed the $2s \rightarrow 1s$, $3s \rightarrow 1s$, $3d \rightarrow 1s$ and $4s,4d \rightarrow 1s$ transitions in silver with better statistical accuracy and, in addition, probed the angular dependence of the photon opening angle θ, verifying the expected ratio of intensities at $\theta = \pi$ and $\theta = \pi/2$. The use of electron capture (Ilakovac et al., 1986, 1991, 1992; Schäffer, 1999) to produce the K-vacancies leads to potentially cleaner two-photon spectra, but for the heaviest systems it can be more convenient to use photoionization, particularly with the advent of 3rd generation synchrotron sources which provide tunable beams of high-energy X rays with small spot size.

5.2. Two-photon decay in gold atoms

In work at the APS, the study of heavier systems has begun starting with a measurement of two-photon decay of K-vacancies in gold atoms (Dunford et al., 2003). The vacancies were produced using X-rays from the bending magnet beamline 12-BM of BESSRC. The beamline monochromator used Si(333) and the resulting X-ray beam was delivered to the experimental hutch where a Ge(220) crystal was utilized to select the third order (85.5 keV) and suppress all other orders. In addition, a 2.5-cm-thick Al plate was used upstream of the Ge diffraction crystal to further reduce the first order radiation (28.5 keV). The beam cross section at the target was defined by slits located in the beamline in front of the hutch. Clean-up slits (4-jaw) were located between the Ge diffraction crystal and the target.

A schematic of the apparatus in the target area is shown in Fig. 17. The X-rays were incident on a 2 mg/cm^2 Au target and passed on to a lead-shielded beam dump located downstream of the target. Two shielded Ge detectors arranged at 135° to the beam direction and 90° to each other detected X-rays from the target. Ta shields located between the two detectors suppressed "cross-talk" events in which a fluorescence photon from the target Compton scatters in one detector crystal and the scattered photon is detected in the other crystal. Such events produce coincidences with sum-energies equal to the energies of the single-photon lines and can mimic two-photon decays. Each of the detectors was surrounded by Pb and Pb walls were located in front of and behind the target to cut down on background from scattered X rays.

Two-photon decays can be distinguished by examining coincident events where both photons lie in the continuum between the characteristic K and L X-ray lines. In Fig. 18 we show a sum-energy spectrum subject to the requirement that the individual photons in each detector lie within the window $\Delta E = 27$ keV centered at 33.2 keV (one half the 2s→1s transition energy). This window excludes photons from cascade transitions. The data in Fig. 18 correspond to 66 h of collection time.

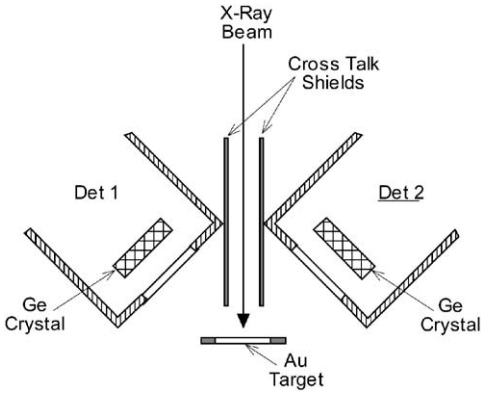

Fig. 17. Schematic of experimental arrangement.

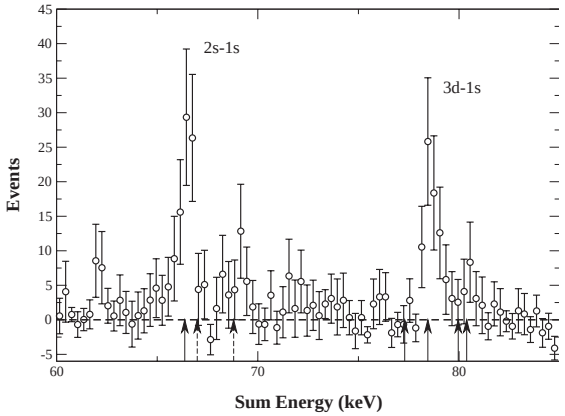

Fig. 18. Sum-energy spectrum of coincidence events. Random coincidences have been subtracted. Error bars are statistical. Solid arrows indicate the sum-energies corresponding to the 2s→1s, 3s→1s, 3d→1s, 4s→1s, and 4d→1s two photon transitions for Au atoms with a single K vacancy. The dashed arrows show the positions of Kα_1 and Kα_2 transition energies.

The sum-energy spectrum of Fig. 18 shows two groups of lines. One group near 66 keV is associated with transitions from $n=2$ to 1s and the other near 78 keV is associated with transitions from $n=3$ to 1s. We analyzed these two regions of the spectrum separately to determine the rate for two-photon events in which the photons shared the transition energy nearly equally. The analysis determined the parameter P, the triply differential two-photon decay rate normalized to the total decay rate for a K-hole W_K (see Ilakovac et al., 1991):

$$P = \frac{1}{W_K}\left(\frac{d^3W}{\hbar d\omega_1\, d\Omega_1\, d\Omega_2}\right). \quad (7)$$

Here $d\Omega j$ are the solid angles of the detectors. The results are presented in Table 1 together with experimental results for other high Z two-photon experiments (Ilakovac et al., 1991, 1992). For xenon we give both theoretical and experimental results and there is good agreement for all transitions except for 3d→1s for which the theory of Tong et al. (1990) provides better agreement.

The measurement of two photon decay in gold atoms has demonstrated the utility of synchrotron radiation for the study of rare processes such as two-photon decay in heavy atoms. With improvements to the experimental setup including better shielding from cross talk and scattered X-ray background and with improved statistics, it will be possible to make a precise determination of the shape of the continuum radiation for the various two-photon decay processes. In addition to improved measurements in Au and heavier atoms, there is also a

Table 1
Comparison of experiment and theory for P at $\omega_1 = \omega_2$ and $\theta = \pi$ in units of $10^{-9}\,\mathrm{keV}^{-1}\,\mathrm{sr}^{-2}$

Transition	$Z = 79$	$Z = 72$	$Z = 54$	TLKP	MC
$2s \rightarrow 1s$	7.80(1.80)	4.54(0.47)	5.91(1.09)	7.13	7.36
$3s \rightarrow 1s$	0.48(0.76)	2.12(0.50)	1.43(0.66)	1.00	0.97
$3d \rightarrow 1s$	6.50(1.14)	5.73(0.64)	6.73(0.95)	6.60	4.85
$(4s + 4d) \rightarrow 1s$	2.47(1.5)	1.36(0.33)	1.33(0.51)	1.42	1.12

The first column ($Z = 79$) shows the results of our experiment. The results for the ns$\rightarrow$1s transitions have been multiplied by 2 and those for the nd$\rightarrow$1s transitions have been multiplied by 14/13, to extrapolate to $\theta = \pi$ in order to compare with the other results in the table which are for back-to-back emission. The correction for the $n = 4$ data was obtained by estimating that 10% of these events were from 4s. The other columns show the hafnium ($Z = 72$) experiment of Ilakovac et al. (1992), and the xenon ($Z = 54$) experiment of Ilakovac et al. (1991). The theoretical results for xenon are in the columns labelled TLKP (Tong et al., 1990) and MC (Mu and Crasemann, 1988).

need for further calculation of two-photon processes in the high Z regime.

6. Search for nuclear excitation by electronic transition (NEET)

In the process of nuclear excitation by electronic transition (NEET), photoionization is used to induce nuclear transitions. The concept of the NEET process was introduced in 1973 by Morita (1973), who pointed out that an atomic inner-shell vacancy might have an observable probability to decay by other than the "normal" modes of X-ray or Auger emission if the decay energy were to match closely an excitation to a state of that atom's nucleus. The associated changes in spin and parity of the atomic and nuclear transitions would also have to match. The energy of the atomic state would be transferred via the exchange of a virtual photon into excitation of the nucleus of that same atom, a process akin to the inverse of internal conversion. The NEET probability, P_{NEET}, is defined as the probability that the decay of the initial excited atomic state will result in the excitation of (and subsequent decay from) the corresponding nuclear state. P_{NEET}, although generally small, is expected to be larger in heavier atoms (more compact atomic wave functions), such as ^{189}Os and ^{197}Au which are considered here. Okamoto (1977) gives a list of heavy atoms where the energy, spin, and parity requirements for atomic and nuclear transitions are simultaneously met and where, therefore, one might possibly detect NEET. Estimates of P_{NEET} for various atomic/nuclear systems have been given by several authors (Morita, 1973; Okamoto, 1977; Harston, 2001; Ho, 1993; Ljubicic, 1991, 1998; Pisk et al., 1989; Sumi and Tanaka, 2000; Tkalya, 1992, 2000). Many of the early estimates involved the use of simplifying approximations that led to unreliable results. Also, it was not recognized at first that P_{NEET} tends to be significantly higher for M1 transitions than for E2 transitions. The involvement of atomic s-states in the M1 transitions leads to a stronger coupling. The more recent calculations (Tkalya, 1992, 2000; Ahmad et al., 2000) give more reliable results.

Early attempts to demonstrate NEET were plagued by severe difficulties which led to spurious results. In the first place, P_{NEET} tends to be small (typically less than 10^{-7}) and therefore one must generate a large number of initial vacancy states. In addition, one must establish that the NEET-excited nuclear state has been populated. This can be done by observing characteristic decay radiation from that state (as in the case of ^{197}Au) or from a lower nuclear state to which the NEET-excited nuclear state decays (as in the case of ^{189}Os). In both cases the decay times of the nuclear states involved can be employed as an additional identification of the nuclear transitions. Finally, one has to be certain that the observed radiation is that which follows NEET transitions and not some other process(es). For example, using particle bombardment to generate the initial atomic vacancy state may also result in the Coulomb or inelastic-scattering excitation of the same state—often much more intensely than that due to NEET. Also, higher-lying nuclear states may be excited, which decay through the "NEET state", mimicking the NEET process. The use of "white" synchrotron or bremsstrahlung photon beams can similarly result in the population of the nuclear "NEET state" or of higher states by resonant nuclear absorption, thereby producing misleading results. The solution (Ahmad et al., 2000; Aoki, 2001; Kishimoto et al., 2000) to these difficulties was to perform the experiments using an intense monochromatic X-ray beam with an energy just above the ionization energy needed to create the initial atomic vacancies, but with the energy carefully chosen not to coincide with excited nuclear states (due attention also being given to the energies of harmonics of the fundamental beam energy).

6.1. NEET experiments on ^{189}Os

Much of the experimental and theoretical work has been dedicated to studies of the third excited state ($5/2^-$) of ^{189}Os, lying at 69.537 keV (Firestone, 1990). This state decays rapidly (1.6 ns) with a partial branch ($\sim 1.2 \times 10^{-3}$) to a lower-lying metastable (6-h half-life) $9/2^-$ state at 30.814 keV, which in turn decays primarily by internal conversion and can readily be measured. In the NEET process involving the 69.537-keV state in ^{189}Os an initial atomic K-vacancy decays via an electronic transition from the M-shell. The KM_I

(70.822 keV, M1), KM_{IV}(71.840 keV, E2), and KM_V (71.911 keV, E2) atomic transitions can contribute. The corresponding nuclear state at 69.537 keV can be excited via M1 or E2 transitions from the $3/2^-$ nuclear ground state. In Ahmad et al. (2000), the following predictions for the NEET probabilities were derived: $P_{NEET}(M1) = 1.3 \times 10^{-10}$, and $P_{NEET}(E2) = 3.8 \times 10^{-13}$.

Experiments on ^{189}Os were performed at Argonne National Laboratory using X-ray beams from a wiggler operated by the Basic Energy Sciences Synchrotron Radiation Center (Montano et al., 1995) at the APS. After initial measurements with a white beam, in which the difficulties with unwanted direct excitation of the nuclei by the X-rays were apparent, Ahmad et al. (2000) used a monochromatic 98.74-keV X-ray beam to produce the K-vacancy states. This beam (5×10^{11} photons/s) was formed by Bragg diffraction from a single (440) Si crystal placed in the wiggler beam. The diffraction angle was $2\theta = 7.5°$. This beam energy was chosen because it lies above the osmium K-edge at 73.9 keV, does not lie near the energy of a nuclear level in ^{189}Os, and corresponds to a convenient and intense diffraction. The energy width of the beam was about 0.1% (100 eV) and the beam-spot size at the target was 0.2-mm wide and 4-mm high. The incident X-ray beam contained a comparably intense component at 49.37 keV (below the osmium K-edge) and also a few-percent component at 148.1 keV. None of the beam components had energies overlapping any of the ^{189}Os nuclear level energies, thereby avoiding problems with nuclear resonant absorption. The decay of the 30.814-keV metastable nuclear state was measured off-line using a Ge (LEPS) detector to count the L X-ray spectrum associated with the L-conversion electrons. The monochromated X-ray beam from the wiggler was incident upon a thin (9.3 mg/cm^2) layer of isotopically separated (95.3%) metallic ^{189}Os electroplated onto a 0.015″-thick Cu disk. Individual targets were irradiated in this fashion for periods of about 20 hours. Large numbers of K-vacancies were produced, some of which were expected to lead via NEET to the 69.5-keV state and thence to the 30.8-keV metastable state of the nucleus. The number of Os K-vacancies generated was monitored by on-line observation of the K X-rays using a Ge detector.

After irradiation the targets were removed and the L X rays associated with decays of the metastable state were detected in a low-background shielded underground counting room where counting with a Ge detector proceeded also for about 20 h. Within the sensitivity of this measurement, there was no evidence of the X-rays that accompany the decay of the ^{189}Os metastable state. Taking into account factors such as the number of K-holes created during the irradiation (and their decay), the branching ratio for feeding the metastable state from the 69.5-keV state, geometrical factors, the emission probability for L X-rays in the isomeric decay, self-absorption in the target, etc, the result $P_{NEET} < 9 \times 10^{-10}$ was obtained (Ahmad et al., 2000). In a subsequent measurement with multiple targets and improved detection sensitivity (Gemmell, 2003), this upper limit was reduced to $P_{NEET} < 3 \times 10^{-10}$. In more recent work at SPring-8, Aoki (2001), using a similar technique found $P_{NEET} < 4.1 \times 10^{-10}$. All of these values are significantly smaller than those obtained in previous measurements and predicted by previous calculations (see a summary in Ahmad et al., 2000). They are, however, consistent with our calculated value of $P_{NEET}(M1) = 1.3 \times 10^{-10}$ and also the recent values calculated by Tkalya (1992, 2000) and by Harston (2001) who obtained $P_{NEET} = 1.2 \times 10^{-10}$ and 1.1×10^{-10} respectively.

6.2. NEET experiment on ^{197}Au

The small value of P_{NEET} in ^{189}Os ($\sim 10^{-10}$), which has made the process undetectable so far, is mainly due to the poor energy matching between the nuclear and atomic transitions. The mismatch is about 1.3 keV, or about 2% of the transition energy. A much more favorable case is found in ^{197}Au, where the energy of the transition from the $3/2^+$ nuclear ground state to the 77.351-keV $1/2^+$ first excited state differs by only 51 eV (0.07%) from that of the $K \rightarrow M_I$ atomic hole transition. Both transitions are M1/E2. However, the excited nuclear state has a half-life of only 1.91 ns (Chunmei, 1991) and so the decay radiation from the state (mainly L internal-conversion electrons) is extremely difficult to measure in a situation where the prompt background radiation from a synchrotron is overwhelming. The group of Kishimoto et al. (2000) have recently succeeded in making the first convincing observation of NEET. This group exploited the pulsed nature of a monochromatic (80.989-keV) X-ray beam from an undulator at SPring-8 to measure P_{NEET} for ^{197}Au. The pulses were of 50 ps duration, spaced 42 ns apart. Using a silicon avalanche diode to detect the internal-conversion electrons from excited nuclei, the group was able to measure time spectra showing the characteristic decay time (2.8 ns) of the 77.351-keV nuclear state. The largest source of background was the very low-level ($\sim 10^{-6}$ of the main bunch intensity) occupation of beam "buckets", spaced about 2 ns apart during the 42-ns periods between the main bunches. The NEET probability was found to be $P_{NEET} = 5.0(6) \times 10^{-8}$. This is in good agreement with the recently calculated values of Tkalya (2000) who found 3.8×10^{-8} and Harston (2001) who reported 3.6×10^{-8}. It is also in fair agreement with the results of Ljubicic (1998) and Sumi and Tanaka (2000) who obtained 7.2×10^{-9} and 1.1×10^{-7} respectively.

The experiment in ^{197}Au provided the first observation of this phenomenon. In the future it is desirable to

observe this process in other systems to provide a thorough test of the theory. In particular, it would be satisfying to finally observe NEET in ^{189}Os where there has been a good deal of effort both theoretically and experimentally.

7. Future

As these examples demonstrate, the third-generation synchrotron sources have been vital to studies of higher-order processes in X-ray photoionization and decay. These studies, while inherently interesting from the point of view of fundamental atomic physics, are of increased practical importance with the current planning for fourth-generation sources which will provide intense short pulses of hard X rays. In particular, the onset of strong field effects with such beams will make higher-order multiphoton processes dominant (see, e.g. Kornberg et al., 2002). Thus, these present studies offer a glimpse of the exciting future of this field.

Acknowledgements

We are immensely grateful to have collaborated in various aspects of this work with I. Ahmad, G.B. Armen, J.-C. Bilheux, M.H. Chen, D.L. Ederer, H. Esbensen, D.S. Gemmell, S. Hasegawa, M. Jung, L. LaJohn, T. LeBrun, J.C. Levin, P.H. Mokler, R.H. Pratt, H. Schmidt-Böcking, W. Schmitt, Th. Stöhlker, and Th. Weber. We thank J. Greene for preparation of the various target samples and the BESSRC staff (M. Beno, M. Engbretson, G. Jennings, G. Knapp, C.A. Kurtz, J. Linton, P.A. Montano, U. Rütt, and C. Wiley) for assistance with the beamlines. This work was supported by the Chemical Sciences, Geosciences, and Biosciences Division and the Advanced Photon Source by the Office of Basic Energy Sciences, Office of Science, US Department of Energy, under Contract No. W-31-109-Eng-38. We also benefitted from a NATO Travel Grant.

References

Åberg, T., 1970. Asymptotic double-photoexcitation cross sections of the helium atom. Phys. Rev. A 2, 1726–1729.

Ahmad, I., Dunford, R.W., Esbensen, H., Gemmell, D.S., Kanter, E.P., Rütt, U., Southworth, S.H., 2000. Nuclear excitation by electronic transition in ^{189}Os. Phys. Rev. C 61, 051304.

Ahopelto, J., Rantavuori, E., Keski-Rahkonen, O., 1979. $K\alpha^h$ hypersatellite spectra in photon excitation and K shell double photoionization cross section for transition metals Ti, Cr, Fe, Ni. Phys. Scr. 20, 71–74.

Amusia, M.Y., 1990. Atomic Photoeffect. Plenum, New York.

Amusia, M.Y., Drukarev, E.G., Gorshkov, V.G., Kazachkov, M.P., 1975. Two-electron photoionization of helium. J. Phys. B: At. Mol. Phys. 8, 1248–1266.

Amusia, M.Y., Baltenkov, A.S., Chernysheva, L.V., Felfli, Z., Msezane, A.Z., 2001. Nondipole parameters in angular distributions of electrons in photoionization of noble-gas atoms. Phys. Rev. A 63, 052506.

Andersson, L., Burgdörfer, J., 1993. Excitation ionization and double ionization of helium by high-energy photon impact. Phys. Rev. Lett. 71, 50–53.

Andersson, L., Burgdörfer, J., 1994a. Excitation ionization and double ionization of helium by Compton scattering. Phys. Rev. A 50, R2810–R2813.

Andersson, L., Burgdörfer, J., 1994b. Single and double ionization of helium by high-energy photon impact. Nucl. Instrum. Methods B 87, 167–172.

Aoki, K., 2001. Probability of nuclear excitation by electron transition in Os atoms. Phys. Rev. C 64, 044609.

Azuma, Y., Berry, H.G., Gemmell, D.S., Suleiman, J., Westerlind, M., Sellin, I.A., Woicik, J.C., Kirkland, J.P., 1995. Attenuation of photons at 3–14 keV energies in helium. Phys. Rev. A 51, 447–453.

Bambynek, W., Crasemann, B., Fink, R.W., Freund, H.-U., Mark, H., Swift, C.D., Price, R.E., Rao, P.V., 1972. X-ray fluorescence yields, Auger, and Coster-Kronig transition probabilities. Rev. Mod. Phys. 44, 716–813.

Bannett, Y., Freund, I., 1982. Two-photon X-ray emission from inner-shell transitions. Phys. Rev. Lett. 49, 539–542.

Bannett, Y.B., Freund, I., 1984. Two-photon inner-shell transitions in molybdenum. Phys. Rev. A 30, 299–308.

Bechler, A., Pratt, R.H., 1989. Higher retardation and multipole corrections to the dipole angular distribution of 1s photoelectrons at low energies. Phys. Rev. A 39, 1774–1779.

Bechler, A., Pratt, R.H., 1990. Higher multipole and retardation corrections to the dipole angular distributions of L-shell photoelectrons ejected by polarized photons. Phys. Rev. A 42, 6400–6413.

Becker, U., Prümper, G., Langer, B., Viefhaus, J., Wiedenhöft, M., Levin, J.C., Sellin, I.A., 1999. Helium double photoionization and Compton scattering: a showcase for electron correlation. Aust. J. Phys. 52, 351–361.

Berger, M.J., Hubbell, J.H., Seltzer, S.M., Coursey, J., Zucker, D., 1999. XCOM: Photon Cross Section Database (version 1.2). National Institute of Standards and Technology, Gaithersburg, MD, NBSIR 87-3597. URL http://physics.nist.gov/PhysRefData/Xcom/Text/XCOM.html.

Bergstrom Jr., P.M., Hino, K., Macek, J., 1995. Two-electron ejection from helium by Compton scattering. Phys. Rev. A 51, 3044–3051.

Berkowitz, J., 2002. Atomic and Molecular Photoabsorption—Absolute Total Cross Sections. Academic Press, San Diego.

Berrah, N., Heiser, F., Wehlitz, R., Levin, J., Whitfield, S.B., Viefhaus, J., Sellin, I.A., Becker, U., 1993. Probing electron correlations in double photoionization of He at intermediate energies. Phys. Rev. A 48, R1733–R1736.

Berry, H.G., Dunford, R.W., Livingston, A.E., 1993. Comparisons of the QED and relativistic parts of the triplet-state energies in the heliumlike sequence. Phys. Rev. A 47, 698–701.

Bethe, H.A., Salpeter, E.E., 1957. Quantum Mechanics of One- and Two-Electron Atoms. Springer, Berlin.

Briand, J.P., Chevallier, P., Tavernier, M., Rozet, J.P., 1971. Observation of K hypersatellites and KL satellites in the X-ray spectrum of doubly K-ionized gallium. Phys. Rev. Lett. 27, 777–779.

Briand, J.P., Touati, A., Frilley, M., Chevallier, P.J., Johnson, A., Rozet, J.P., Tavernier, M., Shafroth, S., Krause, M.O., 1976. The structure of Kα hypersatellite spectra of Cu, Ni and Fe as a test of intermediate coupling. J. Phys. B 9, 1055–1064.

Briand, J.P., Chevallier, P., Chetioui, A., Rozet, J.P., Tavernier, M., Touati, A., 1981. Correlation effects in double-K-vacancy production. Phys. Rev. A 23, 39–45.

Chantler, C.T., 1995. Theoretical form factor, attenuation and scattering tabulation for $Z=1$–92 from $E=1$–10 eV to $E=0.4$–1.0 MeV. J. Phys. Chem. Ref. Data 24, 71–591.

Charpak, G., 1953. Étude experimentale de la double ionisation de la couche K du Mn^{55} lors de la désintégration du Fe^{55} par capture K. Compt. Rend. 237, 243–245.

Chen, M.H., 1991. Auger transition rates and fluorescence yields for the double-K-hole state. Phys. Rev. A 44, 239–242.

Chen, M.H., Crasemann, B., Mark, H., 1982. Effect of the Breit interaction on K X-ray hypersatellite spectra. Phys. Rev. A 25, 391.

Chunmei, Z., 1991. A = 197. Nucl. Data Sheets 62, 433–521.

Cooper, J.W., 1993. Photoelectron-angular-distribution parameters for rare-gas subshells. Phys. Rev. A 47, 1841–1851.

Cooper, J.W., 1996. Total photon attenuation cross sections of helium at energies below 10 keV. An assessment of the accuracy of measured and calculated cross sections. Radiat. Phys. Chem. 47, 927–934.

Cooper, J.W., Manson, S.T., 1969. Photo-ionization in the soft X-ray range: angular distributions of photoelectrons and interpretation in terms of sub-shell structure. Phys. Rev. 177, 157–163.

Crasemann, B. (Ed.), 1985. Atomic Inner-Shell Physics. Plenum, New York.

Crasemann, B., 1996. Photon–atom interactions: 1 keV–1 MeV. In: Drake, G. (Ed.), Atomic, Molecular, and Optical Physics Handbook. American Institute of Physics, Woodbury, NY, pp. 701–711 (Chapter 60).

Derevianko, A., Johnson, W.R., Cheng, K.T., 1999. Non-dipole effects in photoelectron angular distributions for rare gas atoms. At. Data Nucl. Data Tables 73, 153–211.

Diamant, R., Huotari, S., Hämäläinen, K., Kao, C.C., Deutsch, M., 2000a. Cu $K^h\alpha_{1,2}$ hypersatellites: Suprathreshold evolution of a hollow-atom X-ray spectrum. Phys. Rev. A 62, 052519.

Diamant, R., Huotari, S., Hämäläinen, K., Kao, C.C., Deutsch, M., 2000b. Evolution from threshold of a hollow atom's X-ray emission spectrum: The Cu $K^h\alpha_{1,2}$ hypersatellites. Phys. Rev. Lett. 84, 3278–3281.

Dolmatov, V.K., Manson, S.T., 1999. Enhanced nondipole effects in low energy photoionization. Phys. Rev. Lett. 83, 939–942.

Drukarev, E.G., 1995. Breakdown of asymptotics of the double photoionization of helium at the high-energy limit. Phys. Rev. A 51, R2684–R2686.

Drukarev, E.G., Trzhaskovskaya, M.B., 1998. Double photoionization of helium at intermediate photon energies. J. Phys. B: At. Mol. Opt. Phys. 31, 427–448.

Dunford, R.W., Kanter, E.P., Krässig, B., Southworth, S.H., Young, L., Mokler, P.H., Stöhlker, T., 2003. Two-photon decay in gold atoms following photoionization with synchrotron radiation. Phys. Rev. A 67, 054501.

Feinberg, E.L., 1941. Ionization of the atom due to β-decay. J. Phys. (USSR) 4, 423–438.

Firestone, R.B., 1990. A = 189. Nucl. Data Sheets 59, 869–946.

Fisher, C.J., Ithin, R., Jones, R.G., Jackson, G.J., Woodruff, D.P., Cowie, B.C.C., 1998. Non-dipole photoemission effects in X-ray standing wavefield determination of surface structure. J. Phys.: Condens. Matter 10, L623–L629.

Florescu, V., 1984. Two-photon emission in the $3s\rightarrow 1s$ and $3d\rightarrow 1s$ transitions of hydrogenlike atoms. Phys. Rev. A 30, 2441–2448.

Florescu, V., Pătrascu, S., Stoican, O., 1987. Systematic study of 1s–*n*s and 1s–*n*d two-photon transitions of hydrogenlike atoms. Phys. Rev. A 36, 2155–2166.

Forrey, R.C., Sadeghpour, H.R., Baker, J.D., Morgan III, J.D., Dalgarno, A., 1995. Double photoionization of excited ^1S and ^3S states of the helium isoelectronic sequence. Phys. Rev. A 51, 2112–2116.

Forrey, R.C., Yan, Z.-C., Sadeghpour, H.R., Dalgarno, A., 1997. Single and double photoionization from dipole response function. Phys. Rev. Lett. 78, 3662–3665.

Freedman, M.S., 1974. Atomic structure effects in nuclear events. Annu. Rev. Nucl. Sci. 24, 209–247.

Freund, I., 1973. Two-photon emission of X rays. Phys. Rev. A 7, 1849–1853.

Gemmell, D.S., 2003. Nuclear transitions induced by synchrotron X-rays. In: Bianconi, A., Marcell, A., Saini, N.L. (Eds.), X-ray and Inner-Shell Processes, Vol. 652, Rome, Italy, 24–28 June 2002. AIP, Melville, NY, pp. 239–249.

Goldman, S.P., Drake, G.W.F., 1981. Relativistic two-photon decay rates of $2s_{1/2}$ hydrogenic ions. Phys. Rev. A 24, 183–191.

Guillemin, R., Hemmers, O., Lindle, D.W., Shigemasa, E., Guen, K.L., Ceolin, D., Miron, C., Leclercq, N., Morin, P., Simon, M., Langhoff, P.W., 2002. Nondipolar electron angular distributions from fixed-in-space molecules. Phys. Rev. Lett. 89, 033002.

Harston, M.R., 2001. Analysis of probabilities for nuclear excitation by near-resonant electronic transitions. Nucl. Phys. A 690, 447–455.

Heisenberg, W., 1925. The quantum theory of multiplet structure and the anomalous Zeeman effect. Z. Phys. 32, 841–860.

Hemmers, O., Fisher, G., Glans, P., Hansen, D.L., Wang, H., Whitfield, S.B., Wehlitz, R., Levin, J.C., Sellin, I.A., Perera, R.C.C., Dias, E.W.B., Chakraborty, H.S., Deshmukh, P.C., Manson, S.T., Lindle, D.W., 1997. Beyond the dipole approximation: angular-distribution effects in valence photoemission. J. Phys. B 30, L727–L733.

Hemmers, O., Guillemin, R., Kanter, E.P., Krässig, B., Lindle, D.W., Southworth, S.H., Wehlitz, R., Baker, J., Hudson, A., Lotrakul, M., Rolles, D., Stolte, W.C., Tran, I.C., Wolska, A., Yu, S.W., Amusia, M.Y., Cheng, K.T., Chernysheva, L.V., Johnson, W.R., Manson, S.T., 2003. Dramatic nondipole effects in low-energy photoionization: experimental and theoretical study of Xe 5s. Phys. Rev. Lett. 91, 053002.

Hemmers, O., Wang, H., Focke, P., Sellin, I.A., Lindle, D.W., Arce, J.C., Sheehy, J.A., Langhoff, P.W., 2001. Large nondipole effects in the angular distributions of K-shell photoelectrons from molecular nitrogen. Phys. Rev. Lett. 87, 273003.

Henke, B.L., Gullikson, E.M., Davis, J.C., 1993. X-ray interactions: photoabsorption, scattering, transmission, and reflection at $E = 50$–30000 eV, $Z = 1$–92. At. Data Nucl. Data Tables 54, 181–342.

Hino, K., Ishihara, T., Shimizu, F., Toshima, N., McGuire, J.H., 1993. Double photoionization of helium using many-body-perturbation-theory. Phys. Rev. A 48, 1271–1276.

Ho, Y., 1993. Self-consistent description of X-ray, Auger electron, and nuclear excitation. Phys. Rev. C 48, 2277–2284.

Hubbell, J.H., Veigele, W.J., Briggs, E.A., Brown, R.T., Cromer, D.T., Howerton, R.J., 1975. Atomic form factors, incoherent scattering functions, and photon scattering cross sections. J. Phys. Chem. Ref. Data 4, 471–538.

Ice, G.E., Chen, M.H., Crasemann, B., 1978. Photon-scattering cross sections of H_2 and He measured with synchrotron radiation. Phys. Rev. A 17, 650–658.

Ilakovac, K., Tudorić-Ghemo, J., Bušić, B., Horvat, V., 1986. Double-photon decay in xenon atoms. Phys. Rev. Lett. 56, 2469–2472.

Ilakovac, K., Tudorić-Ghemo, J., Kaučić, S., 1991. Two-photon inner-shell transitions in xenon atoms. Phys. Rev. A 44, 7392–7404.

Ilakovac, K., Horvat, V., Krečak, Z., Jerbić-Zorc, G., Ilakovac, N., Bokulić, T., 1992. Two-photon decay in silver and hafnium atoms. Phys. Rev. A 46, 132–141.

Jackson, G.J., Cowie, B.C.C., Woodruff, D.P., Jones, R.G., Kariapper, M.S., Fisher, C., Chan, A.S.Y., Butterfield, M., 2000. Atomic quadrupolar photoemission asymmetry parameters from a solid state measurement. Phys. Rev. Lett. 84, 2346–2349.

Jenkin, J.G., 1981. The development of angle-resolved photoelectron spectroscopy; 1900–1960. J. Electron Spectrosc. Relat. Phenom. 23, 187–273.

Johnson, W.R., 2000. Private communication. Calculations were made with the same code as in Derevianko et al. (1999).

Johnson, W.R., Cheng, K.T., 2001. Strong nondipole effects in low-energy photoionization of the 5s and 5p subshells of xenon. Phys. Rev. A 63, 022504.

Jung, M., Krässig, B., Gemmell, D.S., Kanter, E.P., LeBrun, T., Southworth, S.H., Young, L., 1996. Experimental determination of nondipolar angular distribution parameters for photoionization in the Ar K and Kr L shells. Phys. Rev. A 54, 2127–2136.

Kabachnik, N.M., Sazhina, I.P., 1996. Non-dipolar effects in angular distributions of photoinduced Auger electrons. J. Phys. B 29, L515–L519.

Kanter, E.P., Dunford, R.W., Krässig, B., Southworth, S.H., 1999. Double K-vacancy production in molybdenum by X-ray photoionization. Phys. Rev. Lett. 83, 508–511.

Kanter, E.P., Krässig, B., Southworth, S.H., Guillemin, R., Hemmers, O., Lindle, D.W., Wehlitz, R., Amusia, M.Y., Chernysheva, L.V., Martin, N.L.S., 2003. E1–E2 interference in the VUV photoionization of He. Phys. Rev. A 68, 012714.

Kanter, E.P., Ahmad, I., Dunford, R.W., Gemmell, D.S., Krässig, B., Southworth, S.H., Young, L., 2004. Double K-photoionization of silver, to be published.

Keski-Rahkonen, O., Saijonmaa, J., Suvanen, M., Servomaa, A., 1977. $K\alpha^h$ hypersatellite spectra and K shell double photoionization cross sections of elemental Mg, V, Cr, Mn, and Fe. Phys. Scr. 16, 105–108.

Kheifets, A.S., Bray, I., 1998. Photoionization with excitation and double photoionization of the helium isoelectronic sequence. Phys. Rev. A 58, 4501–4511.

Kishimoto, S., Yoda, Y., Seto, M., Kobyashi, Y., Kitao, S., Haruki, R., Kawauchi, T., Fukutani, K., Okano, T., 2000. Observation of nuclear excitation by electron transition in ^{197}Au with synchrotron X rays and an avalanche photodiode. Phys. Rev. Lett. 85, 1831–1834.

Ko, S.K., Cho, H.J., Nha, S.K., 1998. X-ray spectroscopy in the EC nucleus. Nucl. Phys. A 641, 49–63.

Kornberg, M.A., Miraglia, J.E., 1993. Double photoionization of helium: use of a correlated two-electron continuum wave function. Phys. Rev. A 48, 3714–3719.

Kornberg, M.A., Miraglia, J.E., 1994. Scaling laws in double photoionization. Phys. Rev. A 49, 5120–5123.

Kornberg, M.A., Miraglia, J.E., 1999. Contribution of the quasifree mechanism to the ratio of double-to-single ionization. Phys. Rev. A 60, R1743–R1746.

Kornberg, M.A., Godunov, A.L., Itza-Ortiz, S., Ederer, D.L., McGuire, J.H., Young, L., 2002. Interaction of atomic systems with X-ray free-electron lasers. J. Synchrotron Radiat. 9, 298–303.

Krässig, B., Jung, M., Gemmell, D.S., Kanter, E.P., LeBrun, T., Southworth, S.H., Young, L., 1995. Nondipolar asymmetries of photoelectron angular distributions. Phys. Rev. Lett. 75, 4736–4739.

Krässig, B., Dunford, R.W., Gemmell, D.S., Hasegawa, S., Kanter, E.P., Schmidt-Böcking, H., Schmitt, W., Southworth, S.H., Weber, T., Young, L., 1999. Compton double ionization of helium in the region of the crosssection maximum. Phys. Rev. Lett. 83, 53–56.

Krässig, B., Kanter, E.P., Southworth, S.H., Guillemin, R., Hemmers, O., Lindle, D.W., Wehlitz, R., Martin, N.L.S., 2002. Photoexcitation of a dipole-forbidden resonance in helium. Phys. Rev. Lett. 88, 203002.

Krässig, B., Bilheux, J.-C., Dunford, R.W., Gemmell, D.S., Hasegawa, S., Kanter, E.P., Southworth, S.H., Young, L., LaJohn, L.A., Pratt, R.H., 2003. Nondipole asymmetries of Kr 1s photoelectrons. Phys. Rev. A 67, 022707.

Krause, M.O., 1969. Photo-ionization of krypton between 300 and 1500 eV. Relative subshell cross sections and angular distributions of photoelectrons. Phys. Rev. 177, 151–157.

Krivec, R., Amusia, M.Y., Mandelzweig, V.B., 2000. High-energy limit of the double-electron photoionization cross section of the helium atom. Phys. Rev. A 62, 064701.

Langhoff, P.W., Arce, J.C., Sheehy, J.A., Hemmers, O., Wang, H., Focke, P., Sellin, I.A., Lindle, D.W., 2001. On the angular distributions of electrons photoejected from fixed-in-space and randomly oriented molecules. J. Electron Spectrosc. Relat. Phenom. 114–116, 23–32.

Levin, J.C., Lindle, D.W., Keller, N., Miller, R.D., Azuma, Y., Berrah, N., Berry, H.G., Sellin, I.A., 1991. Measurement of the ratio of double-to-single photoionization of helium at

2.8 keV using synchrotron radiation. Phys. Rev. Lett. 67, 968–971.

Levin, J.C., Sellin, I.A., Johnson, B.M., Lindle, D.W., Miller, R.D., Berrah, N., Azuma, Y., Berry, H.G., Lee, D.-H., 1993. High-energy behavior of the double photoionization of helium from 2 to 12 keV. Phys. Rev. A 47, R16–R19.

Levin, J.C., Armen, G.B., Sellin, I.A., 1996. Photoionization and Compton double ionization of helium from threshold to 20 keV. Phys. Rev. Lett. 76, 1220–1223.

Levinger, J.S., 1953. Effects of radioactive disintegrations on inner electrons of the atom. Phys. Rev. 90, 11–25.

Lindle, D.W., Hemmers, O., Guillemin, R., 2004. Nondipole effects in photoionization of atoms and molecules. Radiat. Phys. Chem., this issue, doi:10.1016/j.radphyschem.2003.12.009.

Ljubicic, A., 1991. A new look at nuclear excitation in an electron transition. Phys. Lett. B 272, 1–4.

Ljubicic, A., 1998. Excitations of nuclear levels in atomic transitions. In: Chia, S.P., Bradley, D.A. (Eds.), Proceedings of the International Meeting on Frontiers of Physics 1998. World Scientific, Singapore, pp. 133–141.

Lubell, M.S., 1995. The case for synchrotron radiation studies of two-electron ions, atoms, and molecules at the ALS. Nucl. Instrum. Methods B 99, 177–181.

Martin, N.L.S., Thompson, D.B., Bauman, R.P., Caldwell, C.D., Krause, M.O., Frigo, S.P., Wilson, M., 1998. Electric-dipole–quadrupole interference of overlapping autoionizing levels in photoelectron energy spectra. Phys. Rev. Lett. 81, 1199–1202.

McGuire, J.H., Berrah, N., Bartlett, R.J., Samson, J.A.R., Tanis, J.A., Cocke, C.L., Schlachter, A.S., 1995. The ratio of cross sections for double to single ionization of helium by high energy photons and charged particles. J. Phys. B: At. Mol. Opt. Phys. 28, 913–940.

McGuire, J.H., Itza-Ortiz, S., Godunov, A.L., Ederer, D.L., Wang, J., Burgdörfer, J., 2000. Exclusive and inclusive cross sections for Compton scattering from H^- and He. Phys. Rev. A 62, 012702.

Migdal, A., 1941. Ionization of atoms accompanying α- and β-decay. J. Phys. (USSR) 4, 449–453.

Mokler, P.H., Dunford, R.W., 2001. The two-photon decay of the $1s2s\,^1S_0$-like states in heavy atomic systems. Fizika A 10, 105–112.

Mokler, P.H., Dunford, R.W., Kanter, E.P., 2002. The two-photon decay of $1s2s\,^1S_0$ states in heavy He-like atomic systems. AIP Conf. Proc. 652, 273–280.

Montano, P.A., Knapp, G.S., Jennings, G., Gluskin, E., Trakhtenberg, E., Vasserman, I.B., Ivanov, P.M., Frachon, D., Moog, E.R., Turner, L.R., Shenoy, G.K., Bedzyk, M.J., Ramanathan, M., Beno, M.A., Cowan, P.L., 1995. Elliptical multipole wiggler facility at the Advanced Photon Source. Rev. Sci. Instrum. 66, 1839–1841.

Morgan, D.V., Bartlett, R.J., 1999. Single-photon ionization of helium from 4.5 to 12 keV by Compton scattering and the photoelectric effect. Phys. Rev. A 59, 4075–4078.

Morita, M., 1973. Nuclear excitation by electron transition and its application to uranium 235 separation. Prog. Theor. Phys. 49, 1574–1586.

Mu, X., Crasemann, B., 1988. Two-photon transitions in atomic inner shells: a relativistic self-consistent-field calculation with applications to Mo, Ag, and Xe. Phys. Rev. A 38, 4585–4596.

Mukoyama, T., Shimizu, S., 1975. Electron shakeoff accompanying internal conversion. Phys. Rev. C 11, 1353–1363.

Nefedov, V.I., Nefedova, I.S., 2000. Angular distribution of the photoelectrons from solids with account for elastic scattering and non-dipolar transitions: the linearly polarized excitation. J. Electron Spectrosc. Relat. Phenom. 113, 3–7.

Oh, S.D., McEnnan, J., Pratt, R.H., 1976. Analytic calculation of screened photoeffect cross sections. Phys. Rev. A 14, 1428–1436.

Okamoto, K., 1977. Possibility of grasers using nuclear excitation by electronic transition. Laser Interact. Relat. Plasma Phenom. 4A, 283–304.

Oura, M., Yamaoka, H., Kawatsura, K., Takahiro, K., Takeshima, N., Zou, Y., Hutton, R., Ito, S., Awaya, Y., Terasawa, M., Sekioka, T., Mukoyama, T., 2002. Correlative multielectron processes in K-shell photoionization of Ca, Ti, and V in the energy range of 8–35 keV. J. Phys. B 35, 3847–3863.

Pan, C., Kelly, H., 1995. Calculation of the double-photoionization cross section of helium. J. Phys. B: At. Mol. Opt. Phys. 28, 5001–5012.

Parpia, F.A., Johnson, W.R., 1982. Radiative decay rates of metastable one-electron atoms. Phys. Rev. A 26, 1142–1145.

Peshkin, M., 1970. Angular distributions of photoelectrons: consequences of symmetry. Adv. Chem. Phys. 18, 1–14.

Peshkin, M., 1996. Photon beam polarization and non-dipolar angular distributions. In: Atomic Physics with Hard X-rays from High Brilliance Synchrotron Light Sources. Argonne National Laboratory, ANL/APS/TM-16, pp. 207–217.

Pisk, K., Kaliman, Z., Logan, B.A., 1989. Calculation of nuclear excitation in an electron transition. Nucl. Phys. A 504, 103–108.

Pratt, R.H., Ron, A., Tseng, H.K., 1973. Atomic photoelectric effect above 10 keV. Rev. Mod. Phys. 45, 273–325.

Qiu, Y., Tang, J.-Z., Burgdörfer, J., Wang, J., 1998. Double photoionization of helium from threshold to high energies. Phys. Rev. A 57, R1489–R1492.

Reilman, R.F., Manson, S.T., 1979. Photoabsorption cross sections for positive atomic ions with $Z \leqslant 30$. Astrophys. J. Suppl. 40, 815–880.

Ricz, S., Sankari, R., Kövér, A., Jurvansuu, M., Varga, D., Nikkinen, J., Ricsoka, T., Aksela, H., Aksela, S., 2003. Strong nondipole effect created by multielectron correlation in 5s photoionization of xenon. Phys. Rev. A 67, 012712.

Sagurton, M., Bartlett, R.J., Samson, J.A.R., He, Z.X., Morgan, D., 1995. Effect of Compton scattering on the double-to-single photoionization ratio in helium. Phys. Rev. A 52, 2829–2834.

Saloman, E.B., Hubbell, J.H., Scofield, J.H., 1988. X-ray attenuation cross sections for energies 100 eV to 100 keV and elements $Z = 1$ to $Z = 92$. At. Data Nucl. Data Tables 38, 1–197.

Salpeter, E.E., Zaidi, M.H., 1962. Lamb shift excitation energy in the ground state of the helium atom. Phys. Rev. 125, 248–255.

Samson, J.A.R., Greene, C.H., Bartlett, R.J., 1993. Comment on "Measurement of the ratio of double-to-single photoionization of helium at 2.8 keV using synchrotron radiation". Phys. Rev. Lett. 71, 201.

Samson, J.A.R., He, Z.X., Bartlett, R.J., Sagurton, M., 1994. Direct measurement of He^+ ions produced by Compton scattering between 2.5 and 5.5 keV. Phys. Rev. Lett. 72, 3329–3332.

Samson, J.A.R., He, Z.X., Stolte, W., Cutler, J.N., 1996. Multiple ionization of free atoms. J. Electron Spectrosc. Relat. Phenom. 78, 19–24.

Samson, J.A.R., Stolte, W.C., He, Z.-X., Cutler, J.N., Lu, Y., Bartlett, R.J., 1998. Double photoionization of helium. Phys. Rev. A 57, 1906–1911.

Schäffer, H.W., 1999. Two photon decay in atoms and ions. Tech. Rep. Diss. 99-16, GSI.

Schmidt, V., 1992. Photoionization of atoms using synchrotron radiation. Rep. Prog. Phys. 55, 1483–1659.

Schneider, T., Chocian, P.L., Rost, J.-M., 2002. Separation and identification of dominant mechanisms in double photoionization. Phys. Rev. Lett. 89, 073002.

Scofield, J.H., 1973. Theoretical photoionization cross sections from 1 to 1500 keV. UCRL-51326, Lawrence Livermore National Laboratory.

Scofield, J.H., 1990. Angular distribution of photoelectrons from polarized X-rays. Phys. Scri. 41, 59–62.

Shaw, P.S., Arp, U., Southworth, S.H., 1996. Measuring nondipolar asymmetries of photoelectron angular distributions. Phys. Rev. A 54, 1463–1472.

Southworth, S.H., Kanter, E.P., Krässig, B., Young, L., Armen, G.B., Levin, J.C., Ederer, D.L., Chen, M.H., 2003. Double K-shell photoionization of neon. Phys. Rev. A 67, 062712.

Spielberger, L., Jagutzki, O., Dörner, R., Ullrich, J., Meyer, U., Mergel, V., Damrau, M., Vogt, T., Ali, I., Khayyat, K., Bahr, D., Schmidt, H.G., Frahm, R., Schmidt-Böcking, H., 1995. Separation of photoabsorption and Compton scattering contributions to He single and double ionization. Phys. Rev. Lett. 74, 4615–4618.

Spielberger, L., Jagutzki, O., Krässig, B., Meyer, U., Khayyat, K., Mergel, V., Tschentscher, T., Buslaps, T., Bräuning, H., Dörner, R., Vogt, T., Achler, M., Ullrich, J., Gemmell, D.S., Schmidt-Böcking, H., 1996. Double and single ionization of helium by 58-keV X rays. Phys. Rev. Lett. 76, 4685–4688.

Spielberger, L., Bräuning, H., Muthig, A., Tang, J.Z., Wang, J., Qiu, Y., Dörner, R., Jagutzki, O., Tschentscher, T., Honkimäki, V., Mergel, V., Achler, M., Weber, T., Khayyat, K., Burgdörfer, J., McGuire, J., Schmidt-Böcking, H., 1999. Cross-section ratio of double to single ionization of helium by Compton scattering of 40–100-keV X rays. Phys. Rev. A 59, 371–379.

Starace, A.F., 1982. Theory of atomic photoionization. In: Mehlhorn, W. (Ed.), Handbuch der Physik, Vol. 31. Springer, Berlin, pp. 1–121.

Stern, E.A., 1988. Theory of EXAFS. In: Koningsberger, D.C., Prins, R. (Eds.), X-Ray Absorption: Principles, Applications, Techniques of EXAFS, SEXAFS and XANES. Wiley, New York, pp. 3–51.

Sumi, Y., Tanaka, S., 2000. Dependence of the nuclear excitation by electron transition on the decay rate. Jpn. J. Appl. Phys. 39, 1894–1897.

Surić, T., Pisk, K., Logan, B.A., Pratt, R.H., 1994. Ionization of 2-electron systems by Compton scattering of a photon. Phys. Rev. Lett. 73, 790–793.

Surić, T., Pisk, K., Pratt, R.H., 1996. Charge dependence of the ratio of double to total ionization of a helium-like ion by Compton scattering of a high energy photon. Phys. Lett. A 211, 289–296.

Surić, T., Drukarev, E.G., Pratt, R.H., 2003. Characterization of high-energy photoionization in terms of the singularities of the atomic potential. I. Photoionization of the ground state of a two-electron atom. Phys. Rev. A 67, 022709.

Thomas, T.D., 1984. Transition from adiabatic to sudden excitation of core electrons. Phys. Rev. Lett. 52, 417–420.

Tkalya, E.V., 1992. Nuclear excitation in atomic transitions. Nucl. Phys. A 539, 209–222.

Tkalya, E.V., 2000. Nuclear excitation by electronic transition between atomic shells. In: Dunford, R.W., Gemmell, D.S., Kanter, E.P., Krässig, B., Southworth, S.H., Young, L. (Eds.), X-Ray and Inner-Shell Processes. AIP Conference Proceedings. Vol. 506. AIP, Melville, NY, pp. 486–495.

Tong, X.-M., Li, J.-M., Kissel, L., Pratt, R.H., 1990. Two-photon transitions in atomic inner shells: relativistic and atomic-screening effects. Phys. Rev. A 42, 1442–1449.

Tseng, H.K., Pratt, R.H., Yu, S., Ron, A., 1978. Photoelectron angular distributions. Phys. Rev. A 17, 1061–1079.

Tung, J.H., Ye, X.M., Salamo, G.J., Chan, F.T., 1984. Two-photon decay of hydrogenic atoms. Phys. Rev. A 30, 1175–1184.

Ullrich, J., Moshammer, R., Dörner, R., Jagutzki, O., Mergel, V., Schmidt-Böcking, H., Spielberger, L., 1997. Recoil ion momentum spectroscopy. J. Phys. B: At. Mol. Opt. Phys. 30, 2917–2974.

Vartanyants, I.A., Zegenhagen, J., 2000. Photoelectric scattering from an X-ray interference field. Solid State Commun. 113, 299–320.

Veigele, W.J., 1973. Photon cross sections from 0.1 keV to 1 MeV for elements $Z=1$ to $Z=94$. At. Data Tables 5, 51–111.

Verner, D.A., Ferland, G.J., Korista, K.T., Yakolev, D.G., 1996. Atomic data for astrophysics. II. New analytic fits for photoionization cross sections of atoms and ions. Astrophys. J. 465, 487–498.

Wehlitz, R., Hentges, R., Prümper, G., Farhat, A., Buslaps, T., Berrah, N., Levin, J.C., Sellin, I.A., Becker, U., 1996. Compton double-to-single ionization ratio of helium at 57 keV. Phys. Rev. A 53, R3720–R3722.

Wu, Y.-J., Li, J.-M., 1988. Non-relativistic self-consistent-field calculation of two-photon transitions in atomic inner shells for Xe. J. Phys. B 21, 1509–1517.

Wuilleumier, F., Krause, M.O., 1974. Photoionization of neon between 100 and 2000 eV: single and multiple processes, angular distributions, and subshell cross sections. Phys. Rev. A 10, 242–258.

Yan, M., Sadeghpour, H.R., Dalgarno, A., 1998. Photoionization cross sections of He and H_2. Astrophys. J. 496, 1044–1050.